Abdominal Imaging

Abdom Imaging (2014)
DOI: 10.1007/s00261-014-0224-8

Multimodality imaging of common and uncommon peritoneal diseases: a review for radiologists

Rafael A. Vicens,[1] Madhavi Patnana,[1] Ott Le,[1] Priya R. Bhosale,[1] Tara L. Sagebiel,[1] Christine O. Menias,[2] Aparna Balachandran[1]

[1]Department of Diagnostic Radiology, Unit 1473, The University of Texas MD Anderson Cancer Center, 1515 Holcombe Blvd, Houston, TX 77030-4009, USA
[2]Department of Radiology, Mayo Cinic, 13400 E. Shea Blvd, Scottsdale, AZ 85259, USA

Abstract

Peritoneal disease can be caused by a wide spectrum of pathologies. While peritoneal disease is usually caused by primary or secondary malignancies, benign diseases can occur and mimic malignancies. This article begins with an overview of peritoneal embryology and anatomy followed by a detailed description of the multimodality imaging appearance of peritoneal diseases. Common diseases include peritoneal carcinomatosis, pseudomyxoma peritonei, lymphomatosis, sarcomatosis, and tuberculous peritonitis. The uncommon diseases which cause peritoneal disease include desmoid fibromatosis, desmoplastic small round cell tumor, malignant mesothelioma, well-differentiated mesothelioma, multicystic mesothelioma, papillary serous carcinoma, leiomyomatosis, extramedullary hematopoiesis, inflammatory pseudotumor and amyloidosis. This manuscript will help the radiologist become familiar with the different peritoneal spaces, pathways of spread, multimodality imaging appearance and differential diagnoses of peritoneal diseases in order to report the essential information for surgeons and oncologists to plan treatment.

Key words: Multimodality—Peritoneal disease

Abbreviations

US	Ultrasound
CT	Computed tomography
MRI	Magnetic resonance imaging
PET	Positron emission tomography
PET/CT	Positron emission tomography/computed tomography
PMP	Pseudomyxoma peritonei
GIST	Gastrointestinal stromal tumor
DSRCT	Desmoplastic small round cell tumor
EH	Extramedullary hematopoiesis
IPT	Inflammatory pseudotumor
FDG	Fluorodeoxyglucose
SUV	Standard uptake value

Correspondence to: Rafael A. Vicens; *email:* rafomd@gmail.com

Published online: 20 August 2014

The peritoneum is the serous membrane lining the abdominal cavity. It is a complex structure that includes the omentum and mesentery and divides the abdominal cavity into multiple compartments and potential spaces. The peritoneum's primary functions are to suspend the visceral organs and to act as a conduit for the network of blood vessels, lymphatics, and nerves that supply the abdominal and pelvic organs. Unfortunately, malignant and benign diseases use these same conduits to spread throughout the abdomen and pelvis.

Peritoneal diseases, either primary or secondary, represent a spectrum of entities with different and sometimes overlapping clinical, pathophysiology, and imaging appearances. The prognosis and treatment of each vary considerably. The radiologist plays a fundamental role in the detection and characterization of peritoneal disease along with estimating the overall extent. This information facilitates staging, guides clinical management, and determines prognosis. Estimating disease burden is particularly important for patient selection for peritoneal cytoreductive surgery and hyperthermic intraperitoneal chemotherapy (HIPEC). When appropriate, a multimodality approach combines the strength of each imaging modality, and increases diagnostic accuracy.

In this review, we present an overview of the peritoneal space anatomy and common and uncommon peritoneal diseases. The epidemiology, pathophysiology, and multimodality appearances of each disease are presented in a way to clarify their differences.

Embryology and anatomy

The peritoneum is a complex organ, but begins simply as a single layer of mesothelial cells, from which the ligaments, mesenteries, omentum, and viscera develop. It is a continuous sheet that is designated as the visceral portion which covers the organs and the parietal portion which covers the abdominal wall. Underneath the mesothelium, a submesothelial layer of connective tissue containing lymphatics, blood vessels, collagen, elastic fibers, and fibroblast-like cells nurtures the peritoneum and its organs [1]. Inferior to this layer, the submesothelial space then forms the subperitoneum. The subperitoneum contains and allows for the ligaments, omentum, mesentery, viscera, blood vessels, lymphatics, connective tissues, and retroperitoneum to interconnect. Separating from the mesothelial layer and its subperitoneum is the peritoneal cavity or intraperitoneal space.

An adequate understanding of the embryological development of the peritoneum is essential to comprehend and realize its structure and function. To simplify, the primitive gut first occupies the peritoneal cavity, supported by a dorsal and ventral mesentery. This divides the peritoneal cavity into a right and left compartment. The viscera then develop within and along the dorsal and ventral mesentery. For example, the ventral mesentery houses the development of the liver, while the dorsal mesentery contains the spleen and pancreas (Fig. 1A).

Likewise, the dorsal and ventral mesentery will evolve into the different ligaments, omentum, and mesenteries as they fold and reflect during growth and development (Fig. 1A). The falciform ligament arises from the ventral mesentery, where it attaches the liver to the ventral abdominal wall, for instance. The spleen and pancreas are connected to the posterior abdominal wall by the splenorenal ligament. The spleen is then attached to the stomach by the gastrosplenic ligament. Both splenorenal and gastrosplenic ligaments are the developments of the dorsal mesentery. Continued growth, elongation, rotation, folds, reflections, and cavitation establish additional ligaments and mesenteries to form the adult peritoneal space (Fig. 1B). The radiologist should recognize the expected location of these ligaments and mesenteries as well as their relationship to organs and vascular landmarks (Table 1). By knowing this information, the radiologist can predict spread patterns of peritoneal disease and hence reports the extent of disease in the peritoneal space, as utilized in clinical staging and surgical planning (Figs. 2A–B, 3A–C).

Two major compartments of the peritoneal space are then separated by the development of the transverse mesocolon, which are the supramesocolic and inframesocolic space (Figs. 4A–C, 6). The falciform ligament further divides the supramesocolic space into the left and right supramesocolic space (Fig. 5A–B). A similar development occurs in the inframesocolic space. It is divided into a right and left inframesocolic space by the obliquely oriented small bowel mesentery (Fig. 4B).

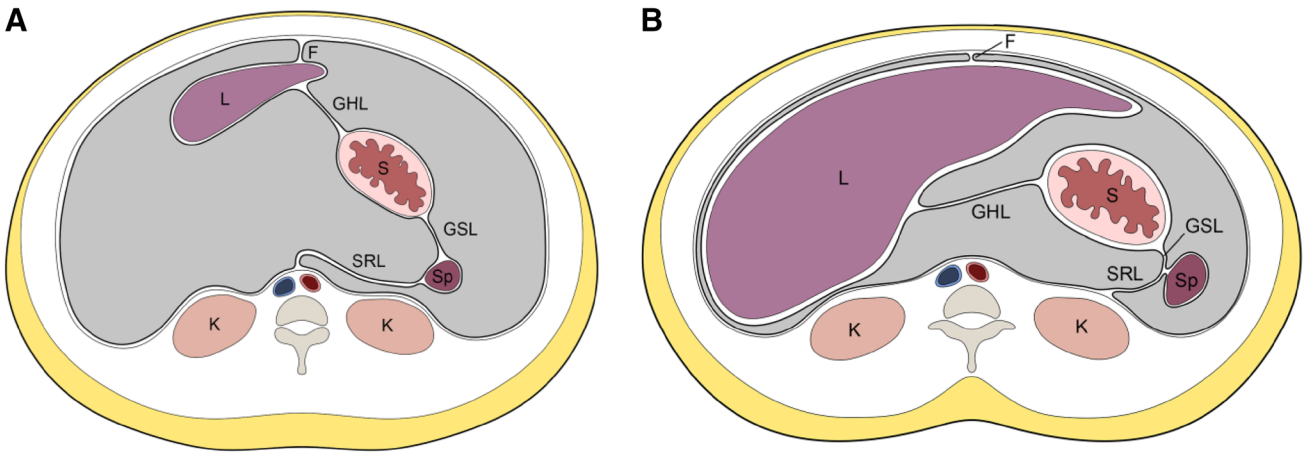

Fig. 1. **A–B** Embryologic development of the primitive gut and peritoneum. The primitive gut consisting of the stomach (*S*) and bowel is suspended in the intraperitoneal cavity and attached to the ventral and dorsal mesentery. The ventral mesentery consists of the falciform ligament (*F*), which connects the liver to the ventral abdominal wall and the gastrohepatic ligament (*GHL*), which in turns connects the liver to the stomach. The dorsal mesentery is made of the gastrosplenic ligament (*GSL*), which connects the stomach to the spleen and the splenorenal ligament (*SRL*), which then attaches the spleen and pancreas to the retroperitoneum/dorsal abdominal wall (**A**). During development and maturation, the liver (*L*) enlarges and rotates to fill the right abdominal cavity (**B**).

Table 1. Ligaments of the adult peritoneum

Ligament	Relation to organs	Landmarks
Gastrohepatic	Lesser curvature of the stomach to the liver	Left gastric vessels
Hepatoduodenal	From the duodenum to the hepatic hilum	Portal vein, proper hepatic artery, extrahepatic bile duct
Gastrocolic	Greater curvature of the stomach to the transverse colon	Perigastric branches of left and right gastroepiploic arteries and veins
Gastrosplenic	Continues to the left of gastrocolic ligament, from greater curvature of stomach to splenic hilum	Short gastric vessels, and left gastroepiploic vessels
Splenorenal	Between spleen and pancreatic tail	Distal splenic artery or proximal splenic vein

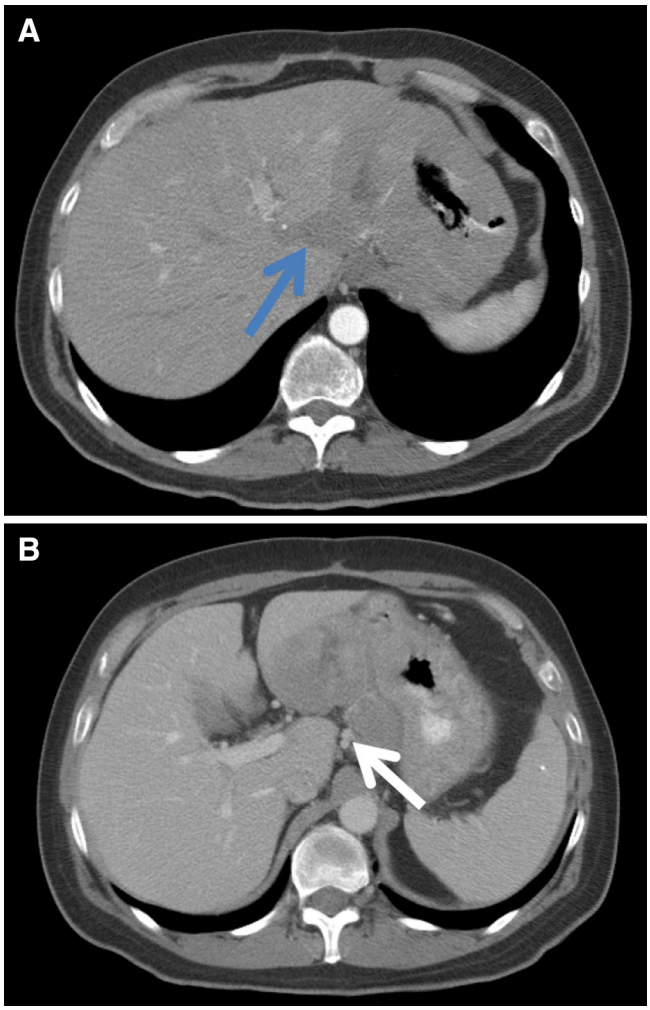

Fig. 2. **A**–**B** A 55-year-old male with history of large B-cell lymphoma. Axial contrast-enhanced CT of the abdomen demonstrates a diffuse infiltrating mass of the stomach extending from the lesser curvature of the stomach into the gastrohepatic ligament (GHL). **A** The GHL is attached superiorly deep within the fissure for the ligamentum venosum (*blue arrow*). **B** The left gastric vessels are a landmark of the GHL (*white arrow*).

The peritoneal development also includes the pelvis, where additional folds, reflections, and spaces are created by the visceral and parietal peritoneum.

Common peritoneal diseases

Peritoneal carcinomatosis

Peritoneal carcinomatosis is the term used to describe metastatic implants in the visceral peritoneal lining from a variety of malignant etiologies. The most common etiologies are malignancies from the colon, rectum, ovaries, stomach, and pancreas. In some instances, however, the tumor may be of unknown origin [2].

Benign etiologies may mimic peritoneal carcinomatosis such as in cases of disseminated peritoneal endometriosis, leiomyomatosis, and tuberculosis [3]. Nonetheless; radiologists should recognize this entity given its significant implications in the staging, management, and prognosis in cases of malignant origin. In addition, the radiologist should try and identify the primary tumor in such instances to help characterize the etiology of the peritoneal involvement.

Peritoneal carcinomatosis presents either focally or diffusely [4]. In the majority of cases, the diffuse type presents with either one of three patterns; the plaque pattern, the nodular (implant) pattern, or the mass-like pattern. These patterns represent a continuous spectrum of spread and/or tumor burden. All patterns result from different pathways implicated in tumor spread such as direct invasion, lymphatic, hematogenous, or intraperitoneal seeding.

The plaque pattern, most commonly seen involving the omentum, is frequently seen with ovarian cancers and usually referred as "caking" of the omentum (Fig. 7A–D). It is commonly associated with higher grade, non-mucinous, and invasive tumors [5]. The nodular and mass-like patterns tend to occur along the serosal peritoneal lining the abdominal cavity, specifically in the subhepatic space, anterior abdominal wall, and cul-de-sac. Both patterns are usually

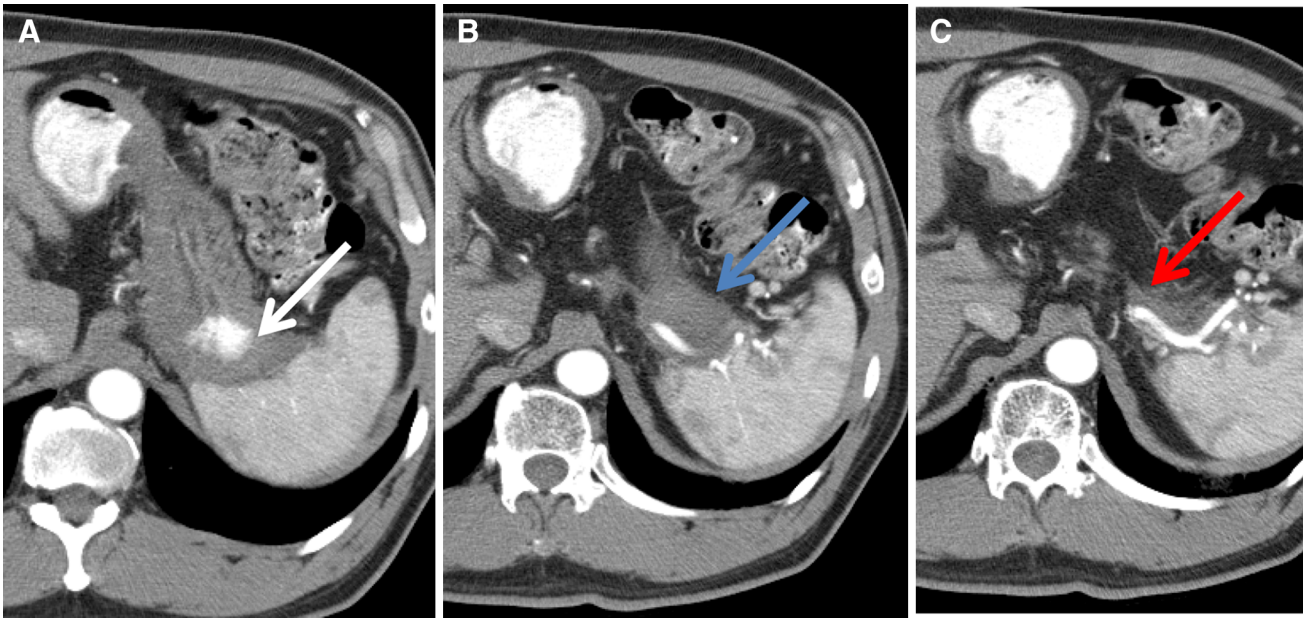

Fig. 3. **A–C** A 59-year-old male with large B-Cell lymphoma. Axial contrast-enhanced CT of the abdomen demonstrates lymphomatous involvement of the stomach (*white arrow*) extending into the splenic hilum involving the gastrosplenic (*blue arrow*) and splenorenal (*red arrow*) ligaments. The splenorenal ligament extends between the spleen and pancreatic tail with the distal splenic artery being a landmark for the splenorenal ligament.

associatedwithlowergrade,mucinous,non-invasivetumors [5].

The sensitivity of abdominal radiographs for detecting peritoneal carcinomatosis is low [6]. When radiographs detect peritoneal carcinomatosis, it is through indirect findings such as ascites, pleural effusions, bulging of flanks, central displacement of small bowel, and indistinct psoas margins. Ultrasound detects hypoechoic masses in cases of omental deposits or iso- to hyperechoic masses when ascites is present [7]. However, ultrasound can be limited in the setting of small volumes of ascites and is operator dependent. Computed tomography (CT) is unquestionably the modality of choice to evaluate peritoneal carcinomatosis. Accurate assessment with CT requires the administration of intravenous and oral contrast. Rectal contrast may be helpful for evaluation of implants near the large bowel and pelvis [8].The sensitivity of CT is dependent on implant size. Archer et al. reported a sensitivity of 25% for lesions smaller than 0.5 cm and 90% for lesions greater than 5 cm. Coakley et al. [9] reported the sensitivity of helical CT for peritoneal tumors <1 cm to be between 25% and 50%. Koh et al. [10] reported that CT detected only 11% of peritoneal implants <0.5 cm from colorectal carcinoma. Direct findings of carcinomatosis include nodular thickening and enhancement of the peritoneum and omental stranding. Indirect findings include ascites and displacement of the small bowel against the mesenteric root.

Optimal evaluation of peritoneal carcinomatosis with magnetic resonance imaging (MRI) requires intravenous Gadolinium, fat suppressed, and gradient echo sequences. [11]. The presentation of peritoneal carcinomatosis on MRI varies depending on tissue composition. Cystic nodules will be hyperintense on T2-weighted images but hypointense on diffusion-weighted images (DWI) [12]. Conversely, solid nodules are expected to be hypointense on T2-weighted images but hyperintense on DWI and enhance following contrast administration [13]. Low et al. [14] reported MRI to be more sensitive than CT for the detection of nodules in the peritoneum and intestinal tract. However, recent advancements in detector technology and new applications of computed tomography are expected to challenge these results. In fact, Marin et al. and Mazzei et al. [15, 16] have shown that using a section thickness and reconstruction interval of no less than 3 mm, in addition to 64-row detectors, improve the sensitivity and positive predictive value of CT detecting peritoneal implants. Moreover, the addition of oral contrast improves the sensitivity of CT to detect small bowel and mesenteric implants [17]. The latter is an important factor since substantial tumor burden in the intestinal tract as well as mesenteric involvement is a relative contraindication to cytoreductive surgery [5].

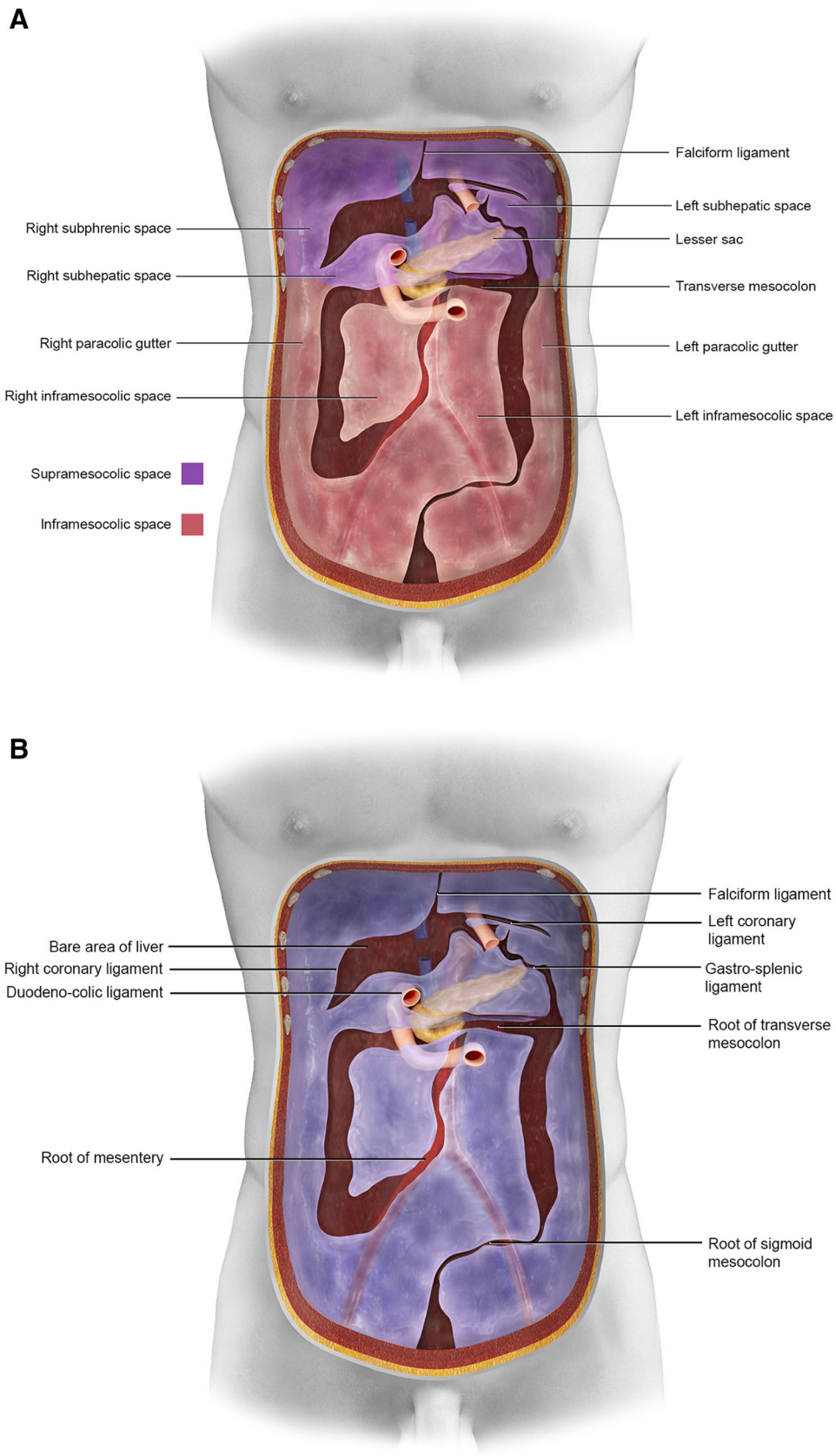

Fig. 4. **A** The transverse mesocolon separates the peritoneal space into a supramesocolic and inframesocolic space. The supramesocolic and inframesocolic spaces are then further subdivided into additional compartments by other ligaments and mesenteries. **B** Relationship of the ligaments and mesenteric attachments about the peritoneal cavity. **C** Omental, mesenteric, and ligamentous attachments as seen on the sagittal view.

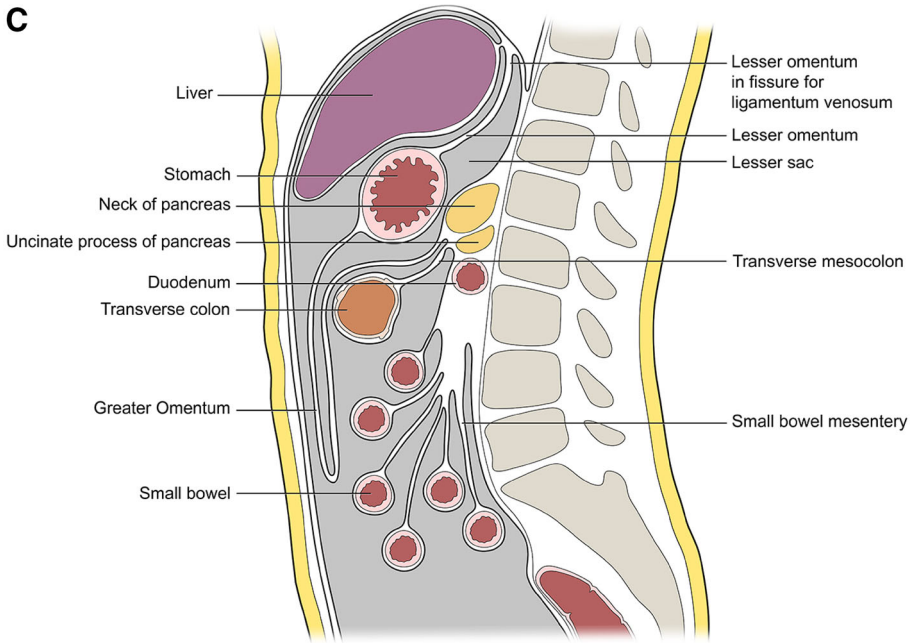

Fig. 4. continued

PET/CT's low sensitivity prevents its routine use for preoperative staging [18]. It can be used to exclude extraperitoneal disease and to confirm extent of peritoneal carcinomatosis in equivocal cases [18]. In addition, PET/CT is helpful in identifying ovarian carcinoma recurrence in patients with negative CT findings and elevated tumor markers [19].

Pseudomyxoma peritonei

Pseudomyxoma peritonei (PMP) or "jelly belly" represents extensive intraperitoneal mucin due to involvement of the peritoneum with from a primary mucinous malignancy most commonly arising from the appendix. The term, however, was first suggested by Werth in 1884, while describing the disease in a woman with mucinous ovarian cancer [20].

Similar to peritoneal carcinomatosis, indirect signs of PMP on abdominal radiography include bulging of flanks, central displacement of small bowel, and indistinct psoas margins. On ultrasound, PMP may present as highly echogenic intraperitoneal fluid. The internal echoes do not change with body position. Multiple echogenic septations in a laminated concentric appearance are pathognomonic [21].

CT findings of PMP include hypodense or cystic masses (<20 Hounsfield Units) with mass effect and scalloping of peritoneal surfaces and visceral organs (Fig. 8A–B). On MRI, the lesion's intensity varies with mucin concentration but in general most are hypointense on T1-weighted images and hyperintense on T2-weighted images. Delayed-enhancing fat-suppressed sequences allow detection of cellular components within the pool of ascites and mucin. Merging conventional MRI protocols plus diffusion-weighted imaging with a *b*-value of at least 400 s/mm^2 improves the sensitivity and specificity for detecting PMP when compared to conventional MRI protocols alone [12, 22].

FDG PET/CT plays a role in establishing extraperitoneal disease in aggressive histological types of PMP, which is a contraindication to cytoreductive surgery [23]. It has been postulated that intense FDG uptake correlates with the most aggressive histological types of PMP, while low levels of FDG uptake correlate with less aggressive forms [23]. Nonetheless, the radiologists must understand the limitation of FDG PET/CT for PMP. The sensitivity decreases with smaller implants or from implants from primary and mucinous tumors resulting in false-negative FDG PET studies due to their low levels of FDG accumulation.

Peritoneal lymphomatosis

Peritoneal lymphomatosis is defined as the intraperitoneal spread of lymphoma. The peritoneal lining lacks lymphoid tissue. The question of how lymphoma invades the peritoneum is controversial. A current theory postulates that lymphoma spreads from bowel epithelium

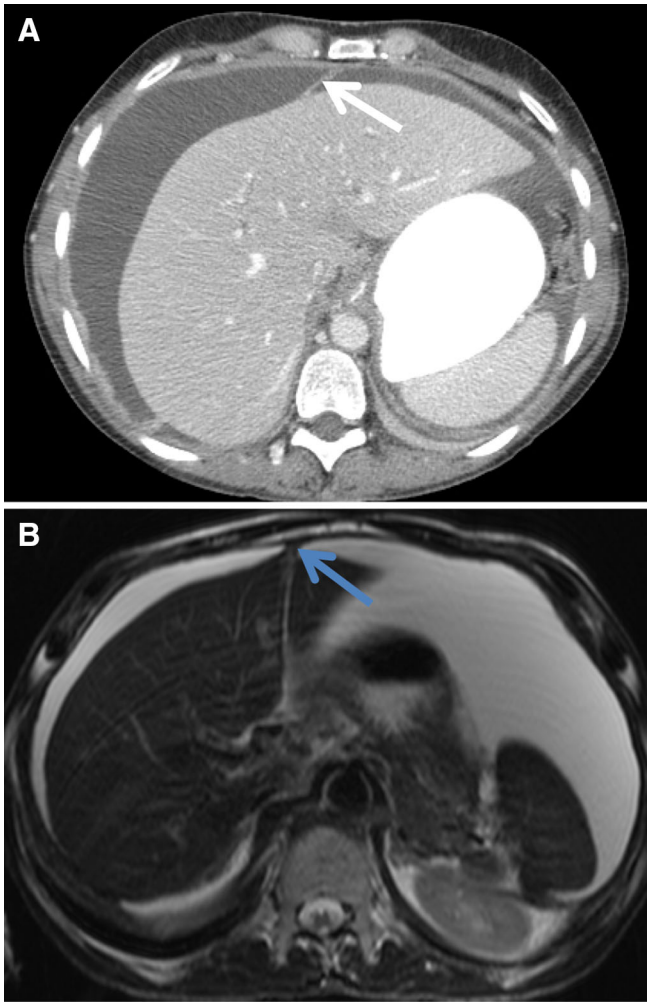

Fig. 5. **A–B** A 51-year-old female with history of primary ovarian serous carcinoma. **A** Axial contrast-enhanced CT of the abdomen demonstrates moderate perihepatic ascites which outlines the falciform ligament (*white arrow*) separating the right and left supramesocolic spaces. **B** Axial T2 turbo spin echo demonstrating the falciform ligament (*blue arrow*).

via ligaments and peritoneal folds. For example, it is believed that, gastric lymphoma reaches the omentum through the gastrocolic ligament and through the transverse mesocolon [24]. Diffuse large B-cell lymphoma and Burkitt's lymphoma are the most common subtypes associated with peritoneal lymphomatosis.

CT findings of peritoneal lymphomatosis include large homogeneous masses and omental caking associated with or without mild-to-moderate ascites (Fig. 9A). Retroperitoneal or mediastinal lymphadenopathy is usually present and should suggest the diagnosis. Additional isolated or complementary findings include enhancement and linear or nodular thickening of the peritoneal lining, omental nodularity, and associated masses in the small bowel or colon [24].

FDG uptake correlates with the aggressiveness of each lymphoma subtype (Fig. 9B) [25]. Thus, in general,

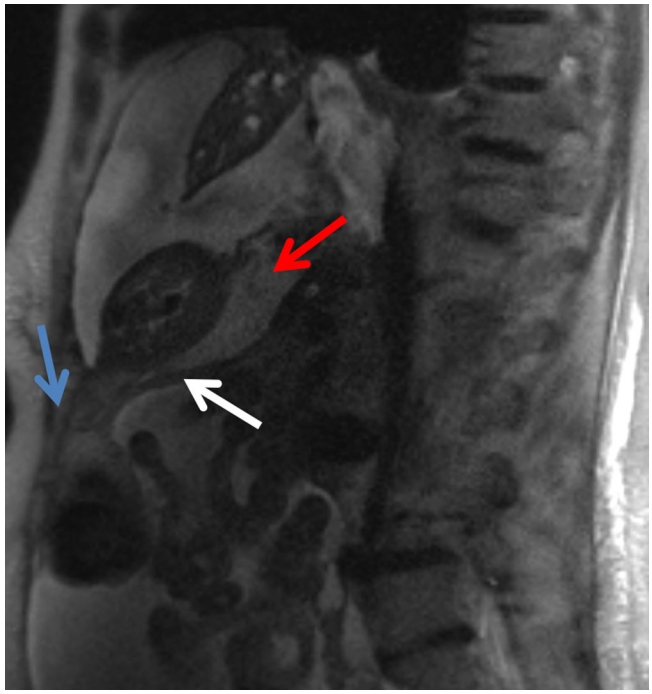

Fig. 6. MRI of greater omentum. Sagittal T2 half-fourier acquisition single shot turbo spin echo (HASTE) image demonstrating the greater omentum (*blue arrow*), as well as the transverse mesocolon (*white arrow*). The lesser sac (*red arrow*) is superior to the transverse mesocolon and posterior to the stomach.

FDG PET/CT is superior to CT in the target selection for biopsy, evaluation of treatment response, and in the detection of malignant transformation from indolent to aggressive lymphomas [26].

Peritoneal sarcomatosis

Peritoneal sarcomatosis is the rare spread of sarcoma to the peritoneum. Sarcomatosis can originate from intra-abdominal sarcomas or extremity sarcomas. The most common sarcomas associated with this entity are gastrointestinal stromal tumor (GIST) and leiomyosarcomas. The imaging characteristics vary depending on the sarcoma type, but in general, there is minimal or no ascites [27].

GIST sarcomatosis presents with multiple, hypervascular, heterogeneous, necrotic lesions with almost no ascites [27] (Fig. 10). Ascites may be seen during therapy with tyrosine kinase inhibitors. Complications of GIST sarcomatosis include gastrointestinal hemorrhage, hemoperitoneum, and fistulization [28].

Peritoneal disease from leiomyosarcoma manifests as bulky masses or peritoneal thickening. The large masses usually heterogeneously enhance and may demonstrate calcifications.

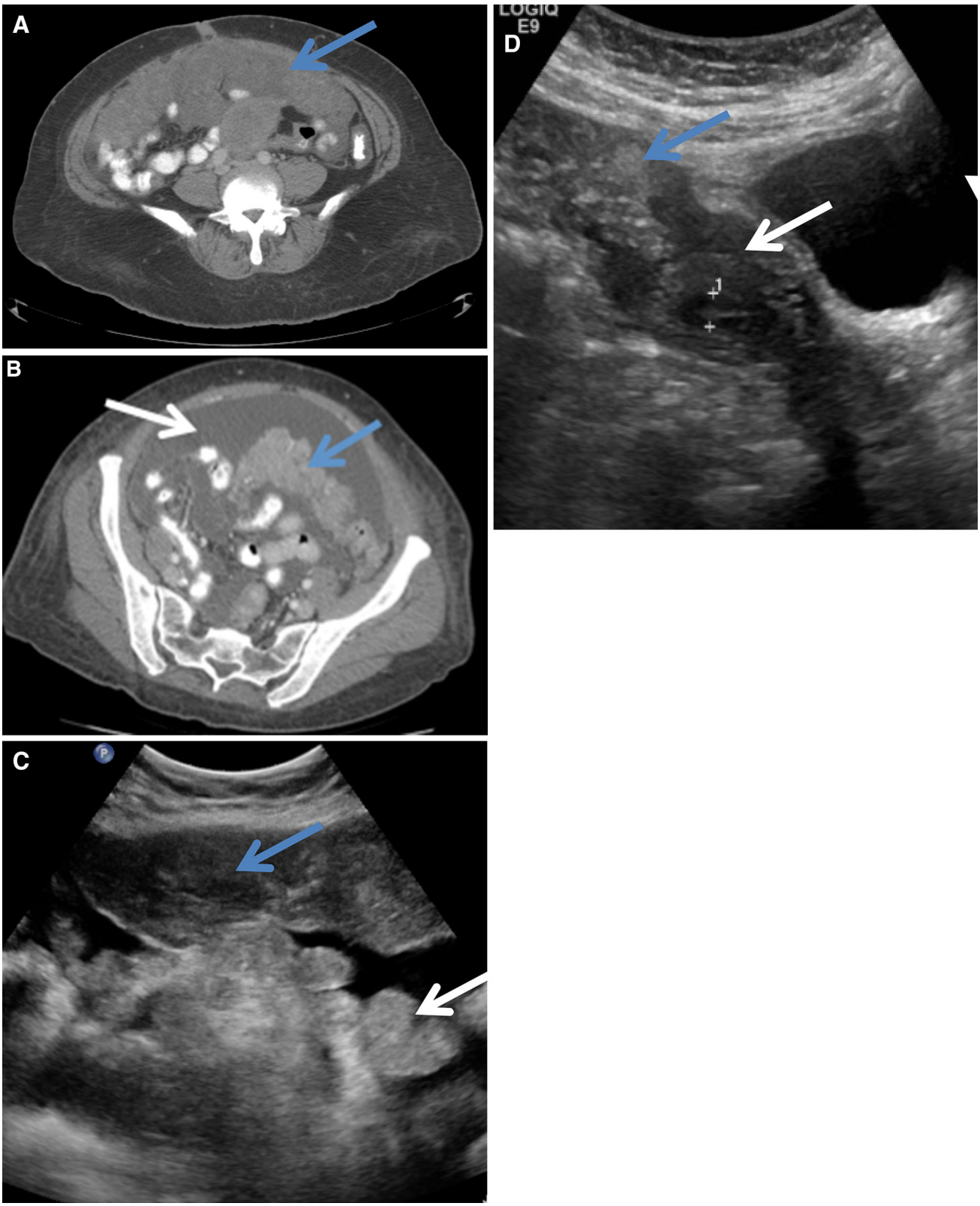

Fig. 7. **A**–**D** 80-year-old female with ovarian serous cystadenocarcinoma and peritoneal carcinomatosis. **A** Axial-enhanced contrast CT demonstrates peritoneal carcinomatosis (*blue arrow*). **B** Inferior slices demonstrate ascites (*white arrow*) and multifocal peritoneal carcinomatosis (*blue arrow*). **C** Transverse Transabdominal US image demonstrates heterogeneous mixed echogenic disease (*blue arrow*) in the anterior abdominal wall. Note ascites separates implants from bowel (*white arrow*). **D** Sagittal transpelvic ultrasound demonstrates peritoneal implants (*blue arrow*) surrounding the uterus (*white arrow*).

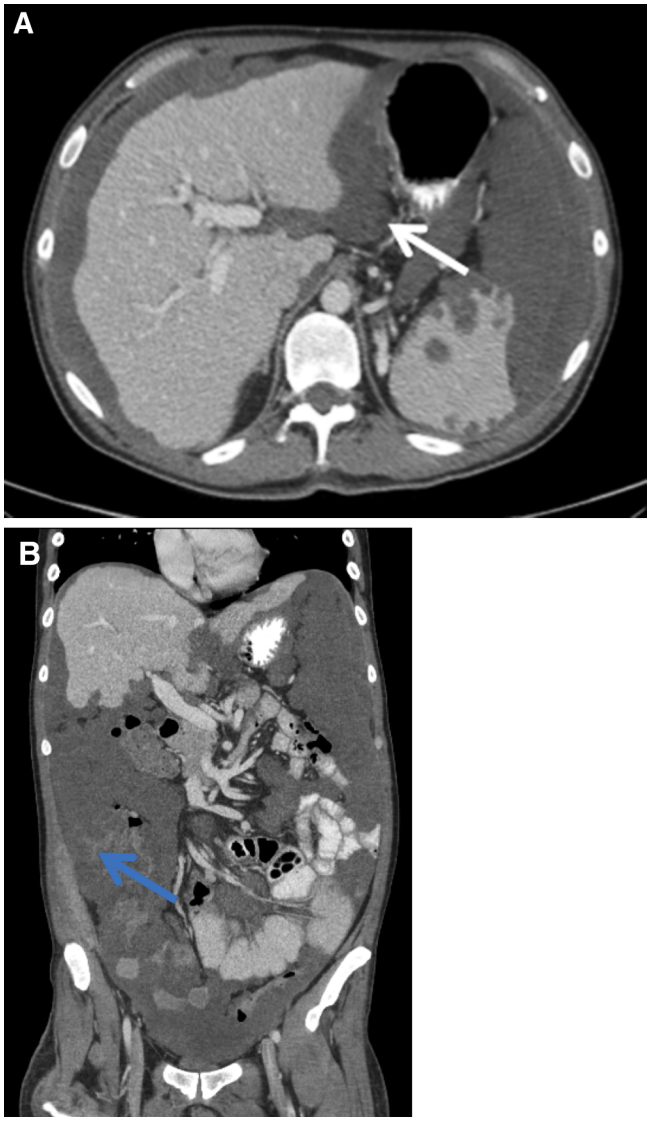

Fig. 8. **A–B** 40-year-old male with well-differentiated mucinous appendiceal adenocarcinoma. **A** Axial contrast-enhanced CT image of the upper abdomen demonstrates low density, cystic implants along the surfaces of the liver and spleen. Note the metastatic implants in the gastrohepatic ligament (*white arrow*). **B** Coronal reformatted CT image demonstrates diffuse metastatic implants also along the small and large bowel mesenteries and along bowel surfaces from pseudomyxoma peritonei (*blue arrow*).

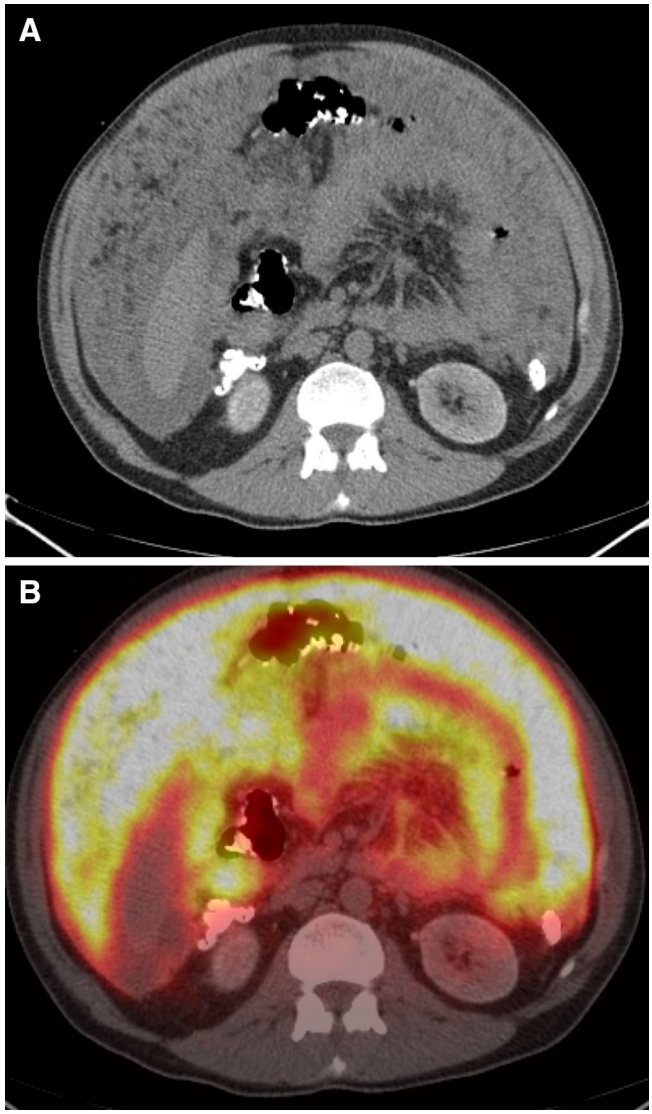

Fig. 9. **A–B** 49-year-old male with Burkitt's lymphoma. **A**, **B** Axial CT and fused PET-CT images demonstrates diffuse omental nodularity and caking from lymphomatosis.

Tuberculous peritonitis

Tuberculous peritonitis is rare. Only 2% of extrapulmonary tuberculosis affects the peritoneum [29]. Many theories explain how Mycobacterium tuberculosis spreads to the peritoneum. The most common theory postulates that peritoneal tuberculosis arises from reactivation of previously established latent foci. Other theories believe in hematogenous spread from remote or near primary sites and/or spilling from involved mesenteric lymph nodes [30].

There are three types of tuberculous peritonitis based on CT and gross appearance that may or may not overlap [31]. The wet type (90%) is characterized by a significant amount of ascites. The ascites may be free or loculated. The attenuation of the fluid is high secondary to the increased protein and cellular content. This is in contrast to ascites from carcinomatosis, where the attenuation is usually low. Chylous ascites has been reported in association with tuberculous peritonitis. The second type is the fibrotic-fixed type (7%). This type is characterized by fixed bowel loops, omental masses, and small volume ascites. The last and least common type is the dry type (3%). In this type, dense peritoneal adhesions, fibrous peritoneal reaction, and caseous nodules are present. The most consistent feature across all types is smooth enhancing thickening of the peritoneal lining

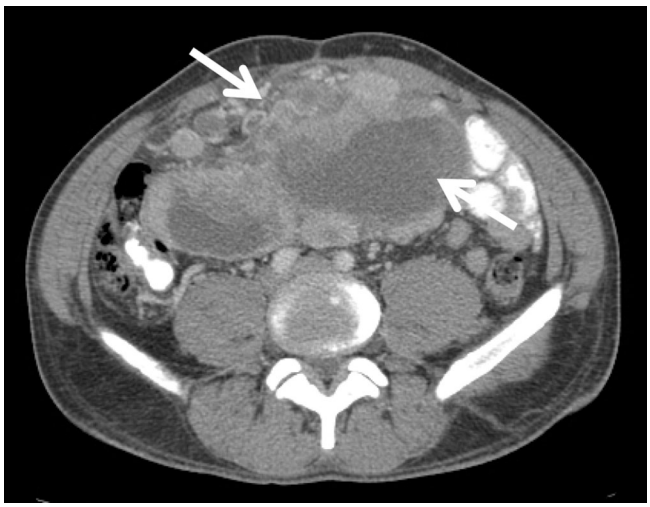

Fig. 10. A 37-year-old male with history of gastrointestinal stromal tumor and peritoneal sarcomatosis. Axial contrast-enhanced CT of the abdomen demonstrates multiple, hypervascular, heterogeneous, necrotic lesions (*white arrows*) in the small bowel mesentery and omentum with no ascites.

(Fig. 11A–B). This feature contrasts with the nodular thickening seen in peritoneal carcinomatosis [29]. Omental caking is almost always absent with tuberculous peritonitis.

On ultrasound, diffuse 2–6 mm peritoneal thickening or tiny nodules less than 5 mm are noted [32]. Enhancement of the exudative ascites may be seen with MRI [30]. Additionally, enhancement and diffusion restriction of the peritoneal lining is expected after Gadolinium intravenous injection (Fig. 12A–D).

FDG PET or PET/CT is not specific for tuberculous peritonitis [33]. However, if performed, delayed images at 2 h can be obtained in order to differentiate carcinomatosis from tuberculosis. Zhuang et al. [34] demonstrated that the mean SUV value of carcinomatosis is higher than inflammation during delayed PET imaging.

Uncommon peritoneal diseases

Desmoid fibromatosis

Desmoid fibromatosis, also known as abdominal desmoids, is a group of benign fibroproliferative tumors. These tumors are locally aggressive and tend to recur locally but do not metastasize [35]. They are classified according to their anatomic location. The most common type is mesenteric fibromatosis. Risk factors for this disease include prior abdominal surgery and the Gardner syndrome variant of familial adenomatous polyposis. Nearly 13% of patients with mesenteric fibromatosis have Gardner syndrome [36].

The main components of desmoids are spindle fibroblast cells, collagen, and myxoid. The imaging

Fig. 11. **A–B** A 55-year-old female with peritoneal tuberculosis. **A**, **B** Axial- and coronal-enhanced contrast CT images demonstrate thickening, enhancement, and nodularity of the peritoneal fascia (*blue arrows*) along with ileocolic adenopathy (*white arrow*).

appearance reflects the combination of these elements. On CT, pure collagen desmoids are homogenous, isodense relative to soft tissue, while pure myxoid desmoids are hypodense [35]. Mixed desmoids demonstrate a striated, whorled appearance reflective of their internal interchanging histological elements. Delayed enhancement is noted with collagenous desmoids, while

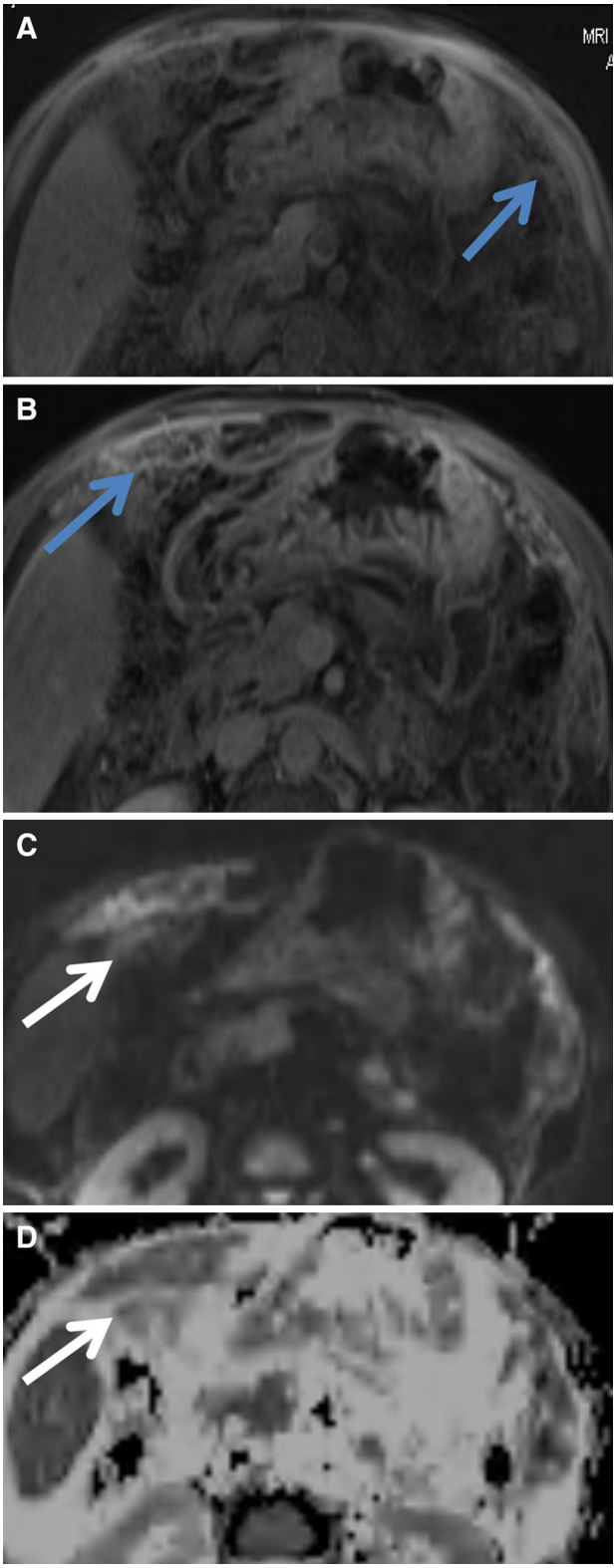

Fig. 12. **A**–**D** 55-year-old African-American male with hepatitis C and new onset ascites and fevers. Pre-(**A**) and post-(**B**) contrast T1 3D VIBE fat-sat images demonstrate ascites with peritoneal/omental enhancement (*blue arrows*). Diffusion-weighted image (**C**) and ADC map (**D**) demonstrate restricted diffusion in the corresponding region (*white arrows*).

minimal or no enhancement is seen with myxoid desmoids [35].

On MRI, collagen components will be iso- to hypointense on T1- and T2-weighted images (Fig. 13A, D). Conversely, myxoid areas will be hypointense on T1-weighted images and hyperintense on T2-weighted images [37]. In both types, there is mild delayed enhancement after intravenous Gadolinium contrast administration (Fig. 13B, C).

The role of FDG PET and PET/CT in these tumors is to define aggressiveness based on FDG uptake, guide biopsy, exclude residual disease after resection, and monitor therapy effects. The FDG uptake is lower than other aggressive peritoneal tumors [38]. Yet, while this difference may be utilized to differentiate desmoid from other tumors, there are reported cases of high FDG uptake mimicking aggressive cancers [39].

Desmoplastic small round cell tumor

Desmoplastic small round cell tumor (DSRCT) is a rare neoplasm that originates from mesothelium. DSRCT demonstrates mesenchymal, epithelial, and neural differentiation [1]. This peculiarity allows pathological diagnosis along with immunohistochemistry. Immunohistochemistry is an important tool to differentiate this entity from other small round cell tumors such as lymphoma, Ewing sarcoma, and neuroblastoma. In the majority of DSRCT cases, desmin, cytokeratin, and vimentin stain positive, with desmin and CK being the most specific [40]. The clinical presentation is usually abdominal pain or an abdominal mass in an adolescent or young adult.

The imaging features consist of bulky, heterogeneous masses in the peritoneal space, predominantly with central necrosis [41] (Fig. 14A–B). On non-enhanced CT images, the masses may have a hyperdense focus reflective of hemorrhage. Minimal arterial heterogeneous enhancement is noted after contrast administration (Fig. 15A–B). No increased enhancement is noted on venous or delayed phases. MRI features include heterogeneous T1 low signal and heterogeneous T2 high signal. After Gadolinium administration, there is heterogeneous contrast enhancement. Subtle hypointense foci sometimes are perceived on T2-weighted images representing desmoplastic reaction. Hyperintense T1 signal and fluid/fluid levels are suggestive with recent hemorrhage in this tumor [42].

FDG PET and PET/CT high sensitivity aids in detecting extraperitoneal metastasis. Generally, this tumor demonstrates heterogeneous FDG uptake (Fig. 15C–D). Zhang et al. [42] reported average SUV values between 5.2 and 12.7. Unfortunately, this is an extremely aggressive tumor with a median survival of 22.3 months from diagnosis, despite cytoreductive surgery and intraperitoneal chemotherapy [43].

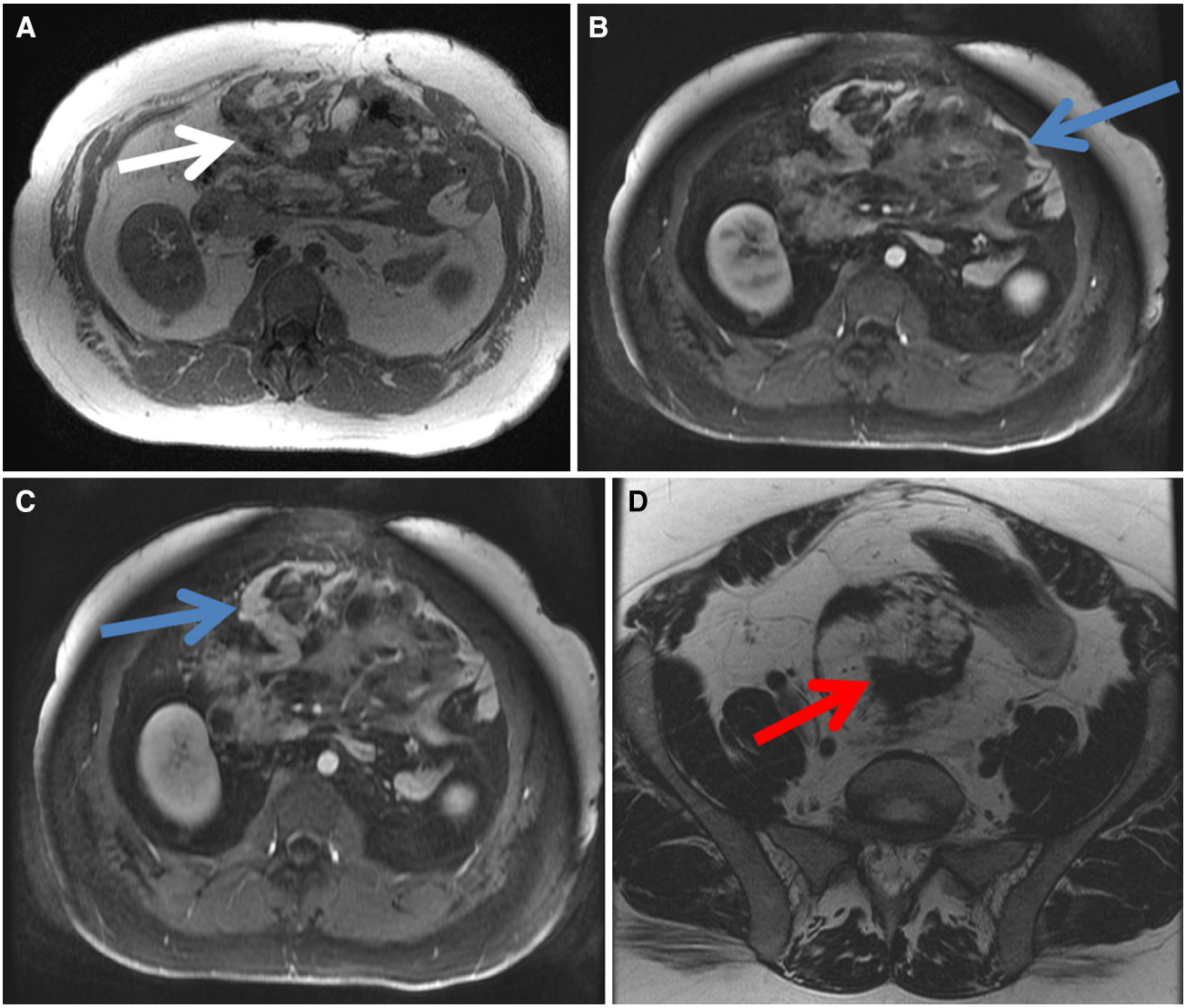

Fig. 13. **A**–**D** A 31-year-old male with history of familial polyposis coli and abdominal desmoid tumor. **A** MRI T1-weighted images without fat saturation of the abdomen demonstrate infiltrating areas in the small bowel mesentery (*white arrow*) isointense to muscle that extend to peritoneal lining. **B**, **C** Post-contrast images with fat saturation demonstrate mild contrast enhancement (*blue arrows*) on delayed imaging. **D** MRI T2-weighted images without fat saturation show low T2 signal areas (*red arrow*) in the small bowel mesentery. These findings are characteristic of desmoid tumors containing pure collagen.

Malignant peritoneal mesothelioma

There are three types of peritoneal mesotheliomas; malignant mesothelioma, well-differentiated mesothelioma, and multicystic mesothelioma [1].

Malignant mesothelioma is the most common form and comprises 6%–10% of all body mesotheliomas [44]. The tumor originates from the superficial layer of mesothelial cells in the peritoneum. Risk factors include exposure of asbestos, therapeutic irradiation, and chronic peritoneal irritation [1]. Asbestos-induced peritoneal mesothelioma is more common in men. The prognosis of this tumor mainly depends on cell morphology and spread pattern [1]. The epithelial cell morphology has a better prognosis than the sarcomatous or mixed types [1]. Likewise, the localized pattern has better prognosis than the diffuse type [1]. The diffuse peritoneal mesothelioma form may present as either infiltrative or with multifocal masses. The diffusely infiltrative type has a worse prognosis [1].

The imaging features of peritoneal malignant mesothelioma do not predict cell morphology [1, 45]. Hence, the role of the radiologist is mainly to describe the pattern, the extent, as well as the complications of this tumor. The diffusely infiltrative type is characterized by the sheet-like or nodular thickening of the peritoneum. Omental caking as well as ascites are usually present.

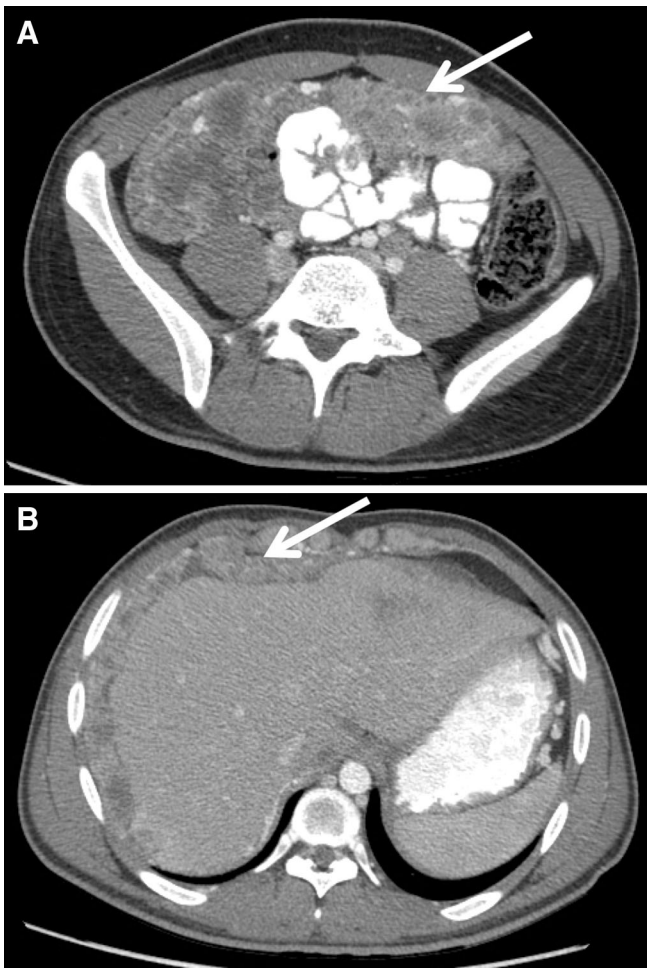

Fig. 14. **A**–**B** A 22-year-old young man with desmoplastic small round cell tumor of the abdomen and pelvis. **A**, **B** Axial CT image after intravenous contrast shows multiple bulky masses (*white arrow*) with central necrosis throughout the perihepatic peritoneal space (*white arrows*).

Straightening and thickening of mesenteric neurovascular bundles have been described [1]. Calcifications and lymphadenopathy are usually absent. MRI features include intermediate-to-low intensity on T1-weighted images (Fig. 16A), intermediate-to-high intensity on T2-weighted images (Fig. 16B) and diffusion restriction (Fig. 16C). The PET/CT appearance of malignant peritoneal mesothelioma has only been described on case reports [46–48]. In the majority of cases, this tumor is FDG avid (Fig. 17A–B). Clinical use PET/CT for malignant pleural mesothelioma is well known [49].

The sensitivity of PET/CT for mesothelioma ranges from 88.2% to 94%, while the specificity ranges from 92.9% to 100% [50, 51]. Shariff et al. [52] concluded that FDG PET differentiates benign from malignant pleural disease, accurately detects recurrence, and provides prognostic information. The extrapolation of these data to malignant peritoneal mesothelioma has yet to be studied.

Well-differentiated peritoneal mesothelioma

This rare subtype typically presents incidentally in woman in their 30 and 40 s undergoing surgery for other reasons [1]. No association exists with asbestos exposure. Microscopically, papillary structures are lined with mesothelial cells with absent or low mitotic activity [53]. The imaging appearance overlaps with other disseminated peritoneal diseases. The CT appearance ranges from a solitary mass to disseminated peritoneal calcified and non-calcified nodules [54]. Presently, the malignant potential of this disease is uncertain. Most cases are indolent but malignant transformation has been reported even after 13 years [55]. For this reason and the possibility of undersampling a malignant mesothelioma, these are often resected.

Multicystic peritoneal mesothelioma

The origin of multicystic peritoneal mesothelioma is controversial. While many believe it is a neoplasm of mesothelial cells, others believe it is an inflammatory reaction of the mesothelium given its high incidence in women with prior pelvic surgery and/or inflammatory diseases [1]. Histologically, clusters of thin-walled cysts are lined by mesothelial cells and filled with eosinophilic serous fluid [1].

Transvaginal or transpelvic ultrasound reveals multiple clusters of anechoic cysts divided by thin wall septations. One or both ovaries entrapped in the cysts are characteristic of this disease [56]. Another entity with similar ultrasound features is the benign peritoneal inclusions cysts. The appearance on CT and MRI overlaps with pseudomyxoma peritonei. Fluid attenuation cysts are perceived on CT disseminated throughout the peritoneal cavity but appear connected (Fig. 18A–B). They do not scallop the visceral organs like pseudomyxoma peritonei [1]. MRI is more sensitive for depicting the cystic nature of this disease especially when small and separated by thick septations [1]. Similar to well-differential peritoneal mesothelioma, the malignant potential of this tumor is unknown. Nonetheless, given reports of recurrence and malignant transformation, most are resected [57, 58].

Peritoneal papillary serous carcinoma

Histologically and immunohistochemically, this tumor is undistinguishable from metastatic serous ovarian carcinoma (Fig. 19A–B). In order to make the diagnosis, the ovaries should be normal in size and the extraovarian sites should be greater than ovarian involvement. If there is involvement of the ovaries, it shall only be limited to the surface epithelium without stromal invasion [1]. Postmenopausal women are typically affected. A few cases reports exist occurring in men [59]. In Chiou's

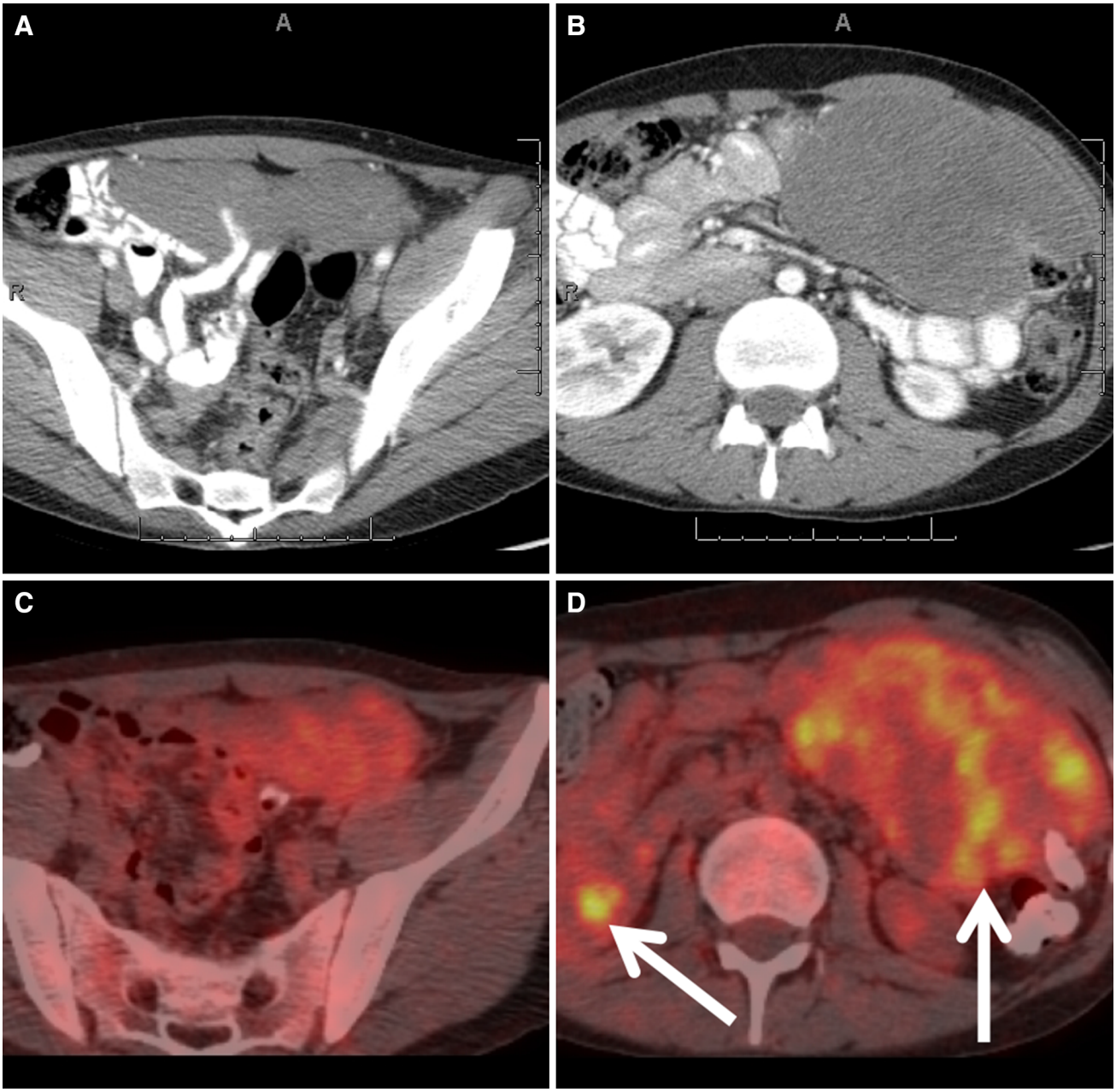

Fig. 15. **A**–**D** A 19-year-old young man with desmoplastic small round cell tumor of the abdomen and pelvis. **A**, **B** Axial CT image after intravenous contrast during the arterial phase demonstrates minimal enhancement of the large masses. **C**, **D** Axial PET/CT images show heterogeneous FDG uptake of the peritoneal implants (*white arrows*).

series of 11 cases, 91% had elevated CA-125 levels, 82% had ascites, 73% had peritoneal nodules or masses, and 64% had omental nodules or masses [60]. Morani et al. [61] case series demonstrated most peritoneal nodules are of low signal intensity on T1-weighted images and high signal intensity on T2-weighted images. Additionally, contrast-enhanced T1-weighted images with fat saturation showed diffuse peritoneal enhancement. PET may be a useful tool for detecting recurrence but up to this date no study has shown its efficacy for detecting this tumor [62].

Disseminated peritoneal leiomyomatosis

Multiple smooth muscle nodules and masses in the peritoneal cavity form this rare disease. The origin is metaplasia of submesothelial smooth muscle [1]. Risk factors include high estrogen levels, uterine leiomyoma, and prior hysterectomy or myomectomy [63]. Because of these risk factors, the incidence is the highest in women of reproductive age, although cases in men and postmenopausal women have been reported [64]. Similar to sarcomatosis, heterogeneous necrotic masses are

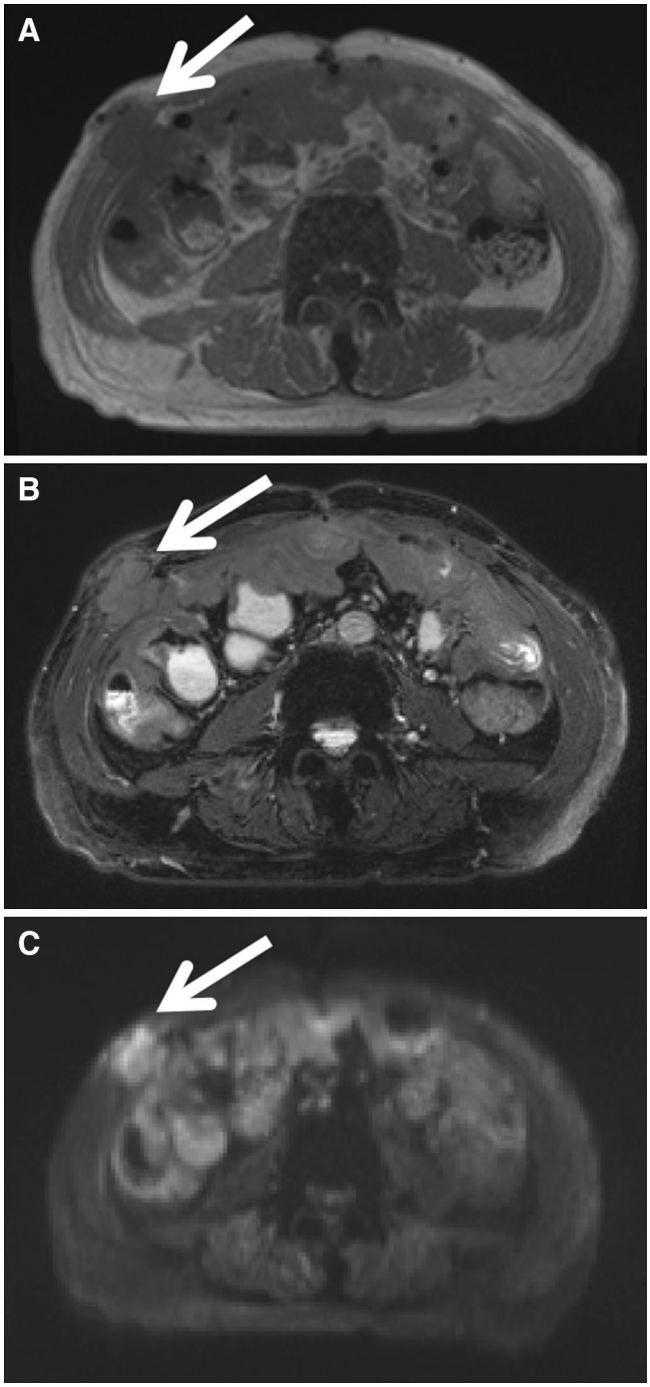

Fig. 16. **A–C** A 50-year-old male with peritoneal mesothelioma. **A**, **B** Axial T1 and T2-weighted image through the mid abdomen demonstrates diffuse peritoneal implants that are isointense to muscle. Note disease is seen extending through a right Spigelian hernia (*white arrows*). **B** Diffusion-weighted images at the same level demonstrate restricted diffusion.

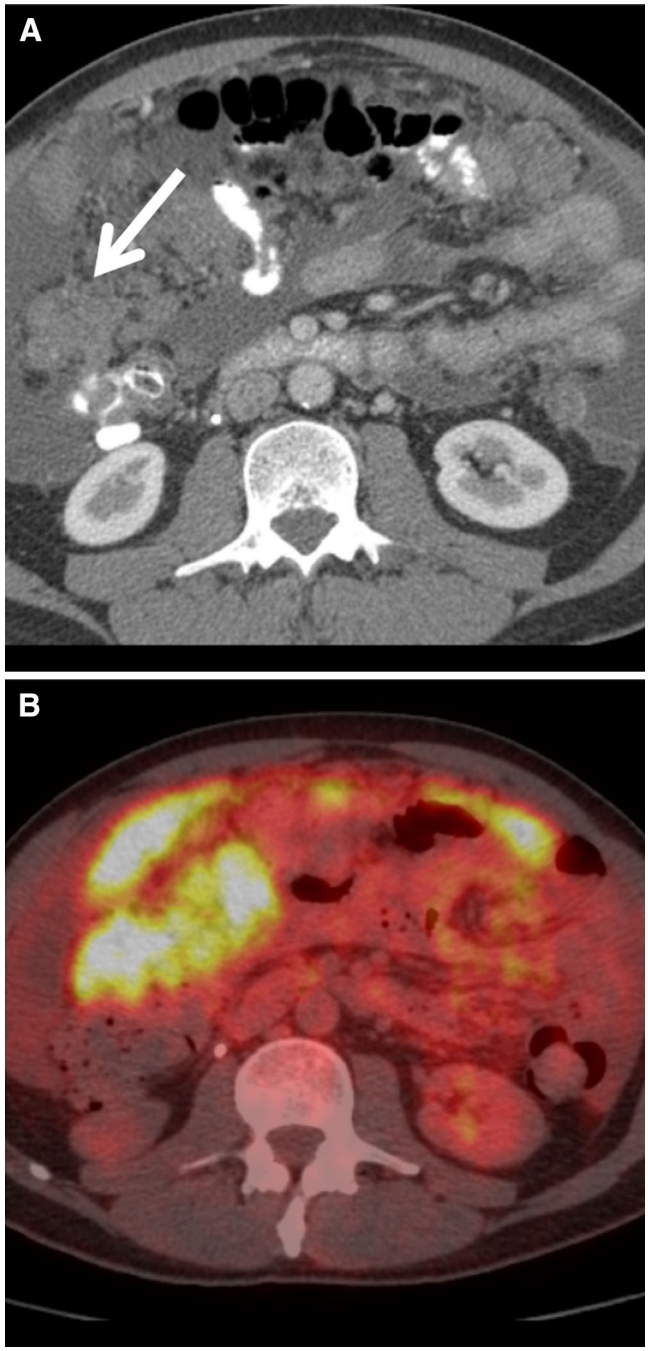

Fig. 17. **A–B** A 63-year old with biopsy proven malignant peritoneal mesothelioma. **A** Axial CT with intravenous contrast during the late arterial phase shows diffuse nodular masses (*white arrow*) and thickening of the peritoneum. **B** Axial fused PET/CT shows the majority of these masses are FDG avid.

noted on CT (Fig. 20A–B). However, ascites and omental caking are almost absent with leiomyomatosis. Furthermore, the nodules and masses appear hypointense on T2-weighted images as oppose to hyperintense on carcinomatosis. The clinical course is general indolent with regression after hormone withdrawal or oophorectomy [63]. Rare cases of sarcomatous transformation are known to occur [65].

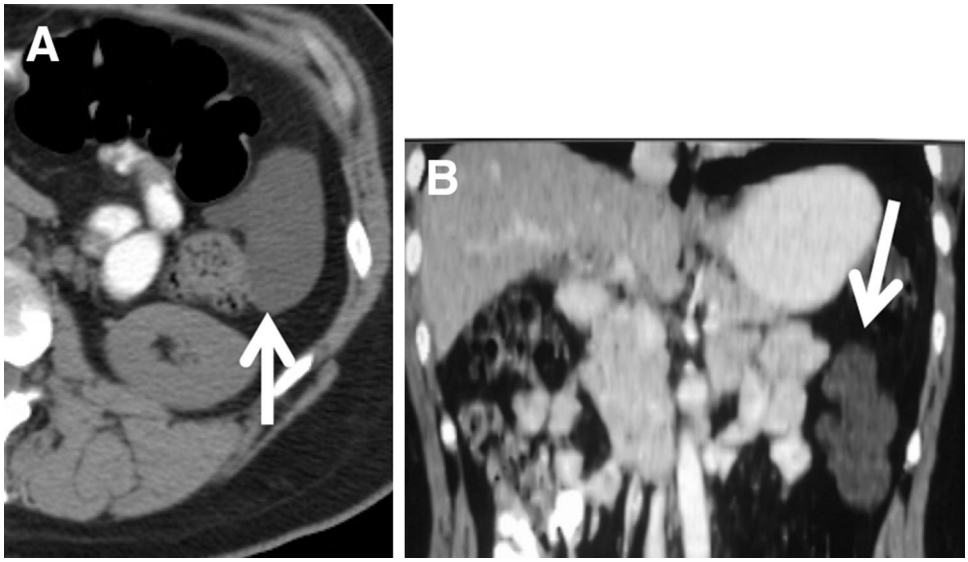

Fig. 18. **A–B** A 47-year-old female with pathologically proven benign cystic mesothelioma. **A** Magnified axial CT image of the left paracolic gutter shows a low attenuated mass with smooth defined margins (*white arrows*). **B** Coronal CT image of the mass shows it is made off multiple connected low attenuated masses.

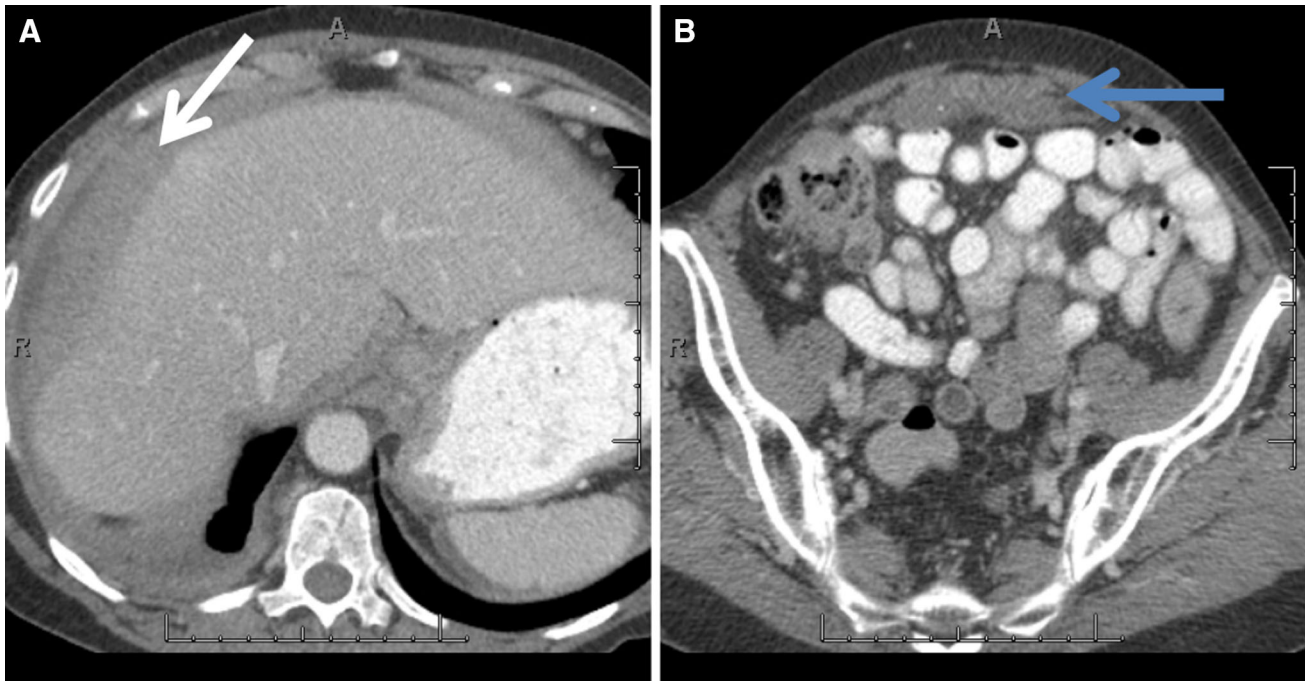

Fig. 19. **A–B** A 56-year-old female with biopsy confirmed peritoneal serous papillary carcinoma. **A** Axial CT with oral and intravenous contrast during the late arterial phase shows diffuse "caking" of the perihepatic peritoneal space (*white arrow*). **B** Axial CT with oral and intravenous contrast demonstrates omental "caking" (*blue arrow*). The appearance of serous papillary carcinoma overlaps with other peritoneal tumors such as carcinomatosis and malignant mesothelioma.

Extramedullary hematopoiesis

Extramedullary hematopoiesis (EH) compensates for blood cell lineage production when the bone marrow is compromised. Common etiologies include myelofibrosis and hemoglobinopathies [66]. It can arise from any mesenchymal tissue. Two forms of EH exist, the infiltrative and the mass-like types. The infiltrative form is the most common (Fig. 21A–B). This type involves visceral organs such as the spleen and liver. The mass-like form usually occurs in the paraspinal compartments [66]. In the peritoneal space, EH diffusely infiltrates the mesentery without bowel retraction or obstruction [67].

The imaging appearance depends on the relative amount of normal marrow components; fat, hemato-

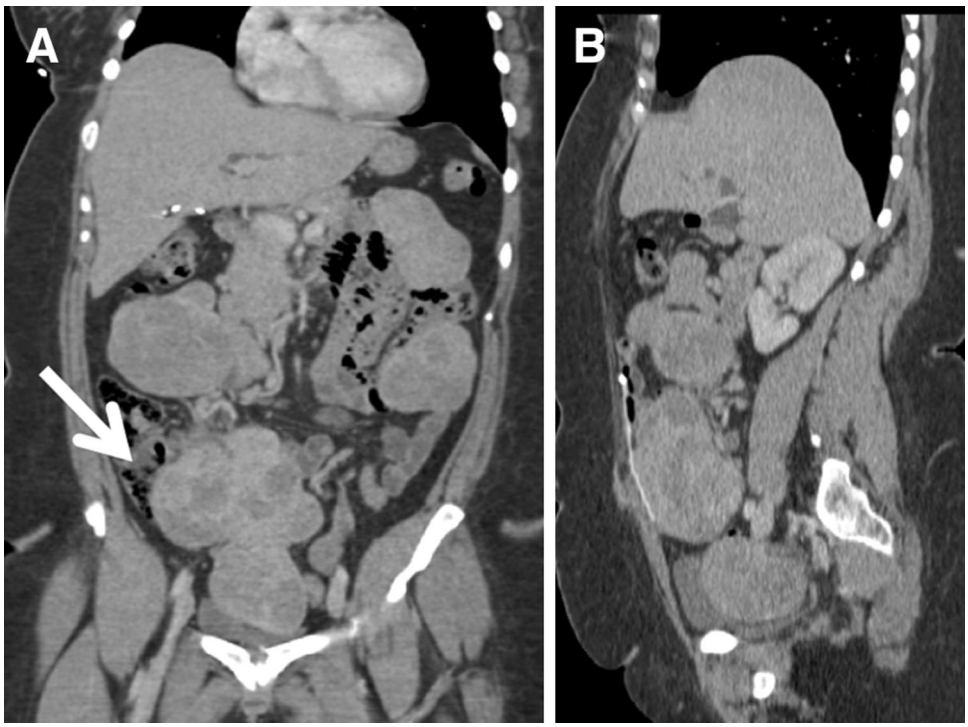

Fig. 20. **A**–**B** A 56-year-old female with disseminated peritoneal leiomyomatosis. **A**, **B** Coronal and sagittal CT images with contrast during the delayed phase demonstrate multiple bulky masses (*white arrow*) in the peritoneal space with a necrotic center and mild peripheral enhancement.

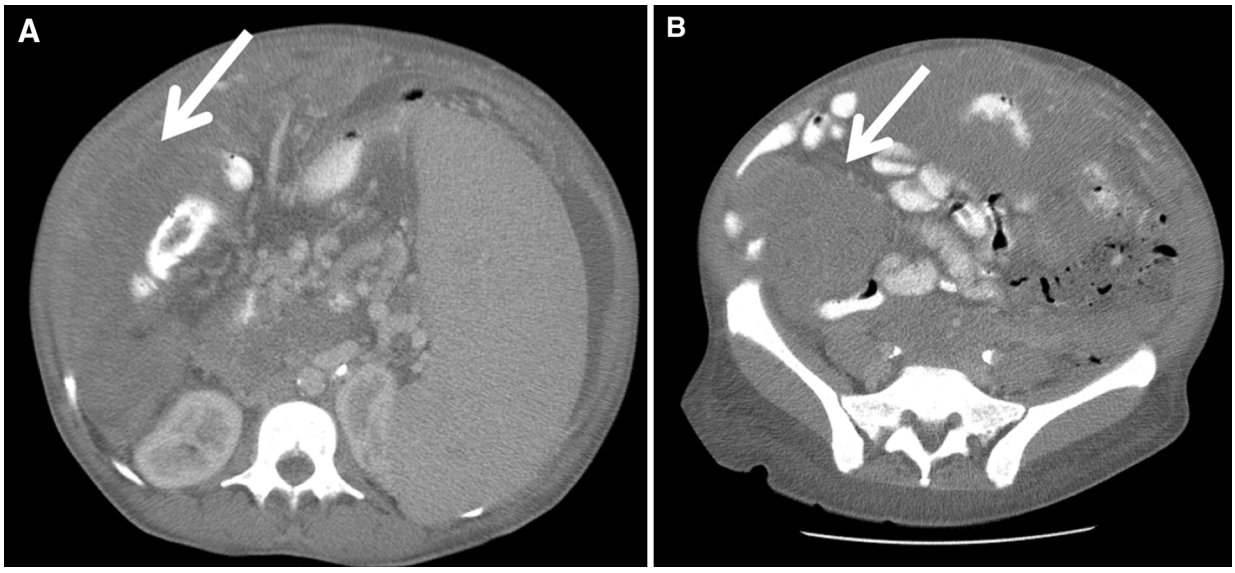

Fig. 21. **A**–**B** A 58-year-old female with myelofibrosis. **A**, **B** Axial contrast-enhanced CT image at the level of the spleen and small bowel mesentery demonstrates splenomegaly and diffuse infiltrative bulky disease (*white arrows*) throughout the peritoneal space and mesentery. Pathology revealed extramedullary hematopoiesis.

poietic cells, and fibrosis. On MRI, the appearance is of intermediate T1 signal intensity and intermediate-to-high T2 signal intensity compared with muscle. Slow early and progressive late enhancement is noted after Gadolinium administration [67]. Ultrasound reveals isoechoic to hypoechoic masses without significant vascularity [67]. CT findings are non-specific and overlap with other disseminated peritoneal diseases

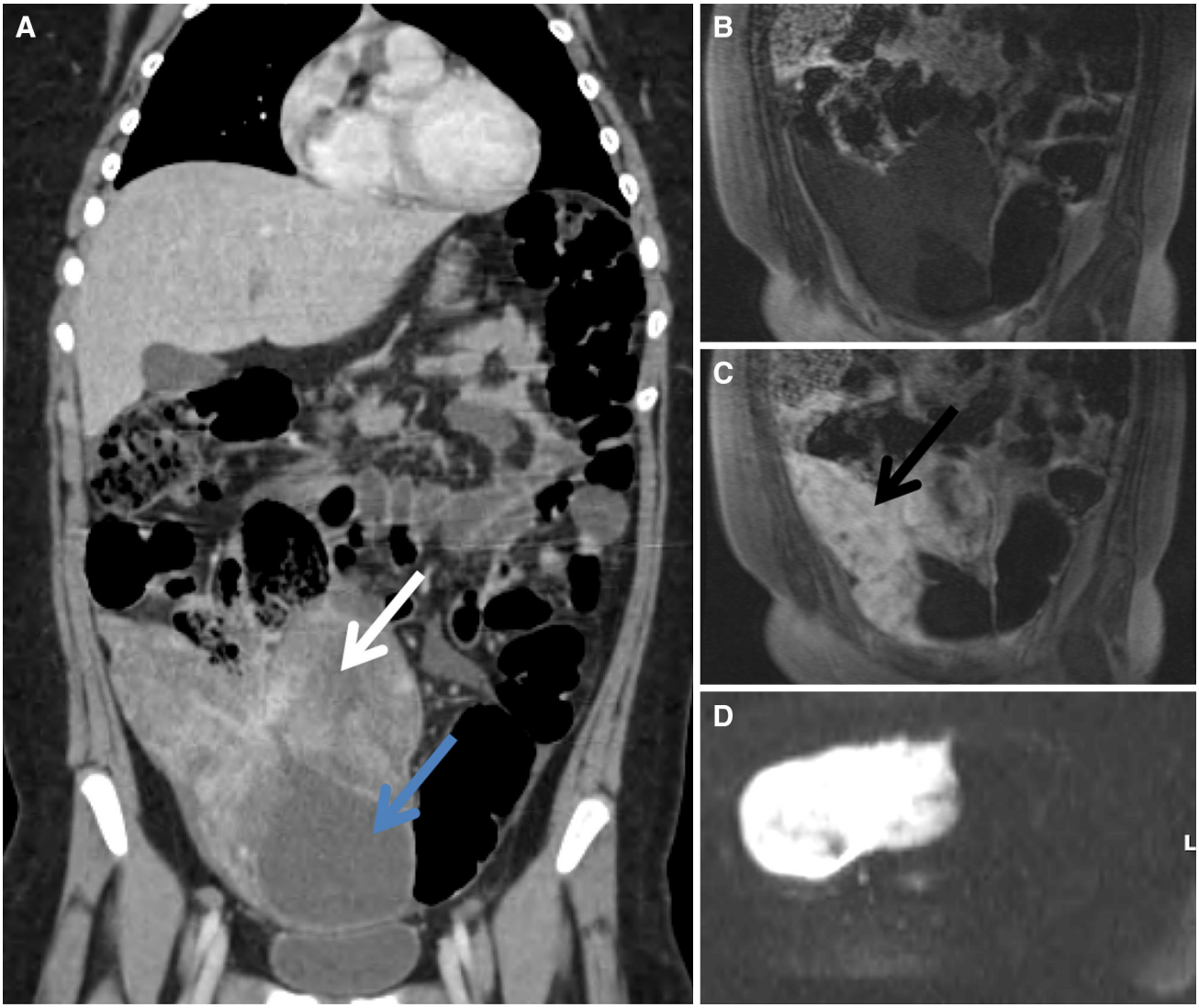

Fig. 22. **A**–**D** An 8-year-old female with a pathologically proven inflammatory pseudotumor of the peritoneum after surgical resection. **A** Coronal CT image with intravenous contrast shows a heterogeneously enhancing mass (*white arrow*) in the right lower abdomen with a predominant solid component and a small cystic component (*blue arrow*). **B** Coronal T1-weighted image with fat saturation shows the mass is diffusely hypointense relative to muscle signal intensity. **C** Coronal T1-weighted image with fat saturation after the administration of Gadolinium-based contrast demonstrates heterogeneous enhancement (*black arrow*). **D** Axial diffusion-weighted image shows the mass demonstrates increased signal. Corresponding ADC map image (not shown) depicts low signal in the mass confirming diffusion restriction.

such as carcinomatosis and malignant peritoneal mesothelioma. The clinical history and the presence of other sites of EH, such as in the liver and spleen, are critical to make this diagnosis.

Inflammatory pseudotumor (IPT)

The etiology of this benign, chronic inflammatory disease is unknown [68]. The imaging manifestations vary from a well-defined mass to an aggressive infiltrative mass.

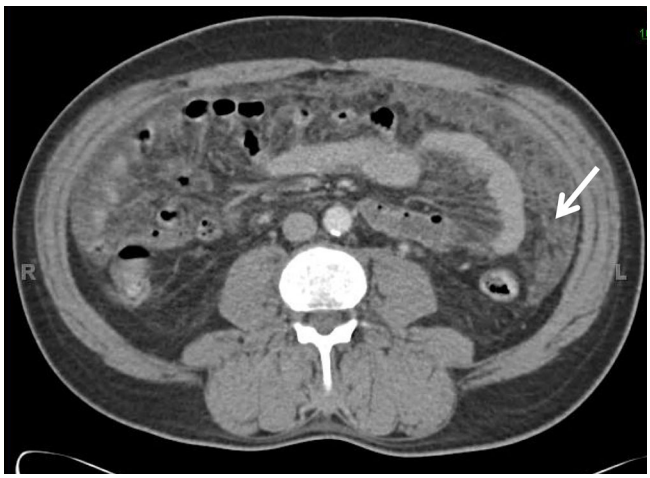

Fig. 23. 58-year-old male with biopsy proven amyloidosis diffusely infiltrating the peritoneal space (*white arrow*) and mesentery without the presence of calcification or small bowel obstruction.

Microscopically, it is composed of a mixture of inflammatory cells and myofibroblastic proliferation [35]. The most common site is the orbit but it can occur anywhere in the body, including the peritoneal space [68]. When in the peritoneal space, the omentum and mesentery are usually involved. On ultrasound, lesions can be hyper or hypoechoic with frequently increased vascularity on Doppler interrogation [69]. CT reveals predominantly hypodense masses or hypodense infiltration of the omentum and mesentery. After contrast administration, there is heterogeneous and progressive enhancement reflective of the underlying fibrotic background (Fig. 22A). A similar enhancement pattern is seen with MRI (Fig. 22B–D). As expected with a predominantly fibrotic mass, there is low signal on T1 and T2-weighted images, a unique feature, only shared with disseminated peritoneal leiomyomatosis. IPT is intensely FDG avid and therefore, indistinguishable from malignant tumors. Treatment of mesenteric IPT is laparoscopic resection as it serves both diagnostic and therapeutic purposes [68].

Amyloidosis

Amyloidosis stems from the abnormal extracellular accumulation of insoluble amyloid proteins in organs and tissues. The amyloid protein is derived from a variety of precursor proteins, such as monoclonal immunoglobulin light chain, which assemble to its peculiar β-pleaded secondary shape. The diagnosis is made with tissue sampling and Congo Stain, where green birefringence is noted under polarized light [70]. Overall, the most common organs involved are the kidneys and the heart. The small bowel is involved 70% of the time in primary amyloidosis [71]. The peritoneum, omentum, and mesentery are rare locations only reported in a small number of case reports [71–73]. The imaging characteristics overlap with other benign and malignant entities. The CT appearance consists of infiltration and nodular thickening of the peritoneal, omental, and mesenteric fat with or without calcifications (Fig. 23). The treatment of amyloidosis depends on the source of proteins. For example, chemotherapy is directed toward plasma cell clone cells when the source of protein is the monoclonal immunoglobulin light chain [70].

Conclusion

Peritoneal diseases represent a diverse group with varied clinical, pathophysiology, imaging appearance, treatment, and prognosis. While many of their imaging features overlap, the radiologist plays a crucial role in diagnosis and staging of the disease. With the understanding of the clinical and pathophysiology of each disease along with the patient's history, the radiologist employing a multimodality approach can improve the diagnostic yield of these dissimilar diseases. Consequently, our reports will be of value guiding appropriate clinical or surgical interventions.

Acknowledgments. David L. Bier for medical illustrations.

References

1. Levy AD, Arnaiz J, Shaw JC, Sobin LH (2008) From the archives of the AFIP: primary peritoneal tumors: imaging features with pathologic correlation. Radiographics 28(2):583–607; quiz 21–22
2. Thomassen I, Verhoeven RH, van Gestel YR, van de Wouw AJ, Lemmens VE, de Hingh IH (2014) Population-based incidence, treatment and survival of patients with peritoneal metastases of unknown origin. Eur J Cancer 50(1):50–56
3. Levy AD, Shaw JC, Sobin LH (2009) Secondary tumors and tumorlike lesions of the peritoneal cavity: imaging features with pathologic correlation. Radiographics 29(2):347–373
4. Raptopoulos V, Gourtsoyiannis N (2001) Peritoneal carcinomatosis. Eur Radiol 11(11):2195–2206
5. Gonzalez-Moreno S, Gonzalez-Bayon L, Ortega-Perez G, Gonzalez-Hernando C (2009) Imaging of peritoneal carcinomatosis. Cancer J 15(3):184–189
6. Bundrick TJ, Cho SR, Brewer WH, Beachley MC (1984) Ascites: comparison of plain film radiographs with ultrasonograms. Radiology 152(2):503–506
7. Park CM, Kim SH, Kim SH, et al. (2003) Recurrent ovarian malignancy: patterns and spectrum of imaging findings. Abdom Imaging 28(3):404–415
8. Archer AG, Sugarbaker PH, Jelinek JS (1996) Radiology of peritoneal carcinomatosis. Cancer Treat Res 82:263–288
9. Coakley FV, Choi PH, Gougoutas CA, et al. (2002) Peritoneal metastases: detection with spiral CT in patients with ovarian cancer. Radiology 223(2):495–499
10. Koh JL, Yan TD, Glenn D, Morris DL (2009) Evaluation of preoperative computed tomography in estimating peritoneal cancer index in colorectal peritoneal carcinomatosis. Ann Surg Oncol 16(2):327–333
11. Low RN (2007) MR imaging of the peritoneal spread of malignancy. Abdom Imaging 32(3):267–283
12. Low RN, Sebrechts CP, Barone RM, Muller W (2009) Diffusion-weighted MRI of peritoneal tumors: comparison with conventional MRI and surgical and histopathologic findings—a feasibility study. AJR Am J Roentgenol 193(2):461–470
13. Iafrate F, Ciolina M, Sammartino P, et al. (2012) Peritoneal carcinomatosis: imaging with 64-MDCT and 3T MRI with diffusion-weighted imaging. Abdom Imaging 37(4):616–627
14. Low RN, Barone RM, Lacey C, et al. (1997) Peritoneal tumor: MR imaging with dilute oral barium and intravenous gadolinium-con-

taining contrast agents compared with unenhanced MR imaging and CT. Radiology 204(2):513–520
15. Marin D, Catalano C, Baski M, et al. (2010) 64-Section multidetector row CT in the preoperative diagnosis of peritoneal carcinomatosis: correlation with histopathological findings. Abdom Imaging 35(6):694–700
16. Mazzei MA, Khader L, Cirigliano A, et al. (2013) Accuracy of MDCT in the preoperative definition of Peritoneal Cancer Index (PCI) in patients with advanced ovarian cancer who underwent peritonectomy and hyperthermic intraperitoneal chemotherapy (HIPEC). Abdom Imaging 38(6):1422–1430
17. Courcoutsakis N, Tentes AA, Astrinakis E, Zezos P, Prassopoulos P (2013) CT-Enteroclysis in the preoperative assessment of the small-bowel involvement in patients with peritoneal carcinomatosis, candidates for cytoreductive surgery and hyperthermic intraperitoneal chemotherapy. Abdom Imaging 38(1):56–63
18. Chang MC, Chen JH, Liang JA, et al. (2013) PET or PET/CT for detection of peritoneal carcinomatosis: a meta-analysis. Clin Nucl Med 38(8):623–629
19. Klumpp B, Schwenzer NF, Gatidis S, et al. (2014) Assessment of relapse in patients with peritoneal carcinomatosis after cytoreductive surgery and hyperthermic intraperitoneal chemotherapy using F-18-FDG-PET/CT. RoFo 186(4):359–366
20. Touloumis Z, Galyfos G, Kavouras N, Menis M, Lavant L (2013) Aggressive pseudomyxoma peritonei: a case report with an unusual clinical presentation. Case reports in oncological medicine
21. Appelman Z, Zbar AP, Hazan Y, Ben-Arie A, Caspi B (2013) Mucin stratification in pseudomyxoma peritonei: a pathognomonic ultrasonographic sign. Ultrasound Obstetr Gynecol 41(1):96–97
22. Bozkurt M, Doganay S, Kantarci M, et al. (2011) Comparison of peritoneal tumor imaging using conventional MR imaging and diffusion-weighted MR imaging with different b values. Eur J Radiol 80(2):224–228
23. Passot G, Glehen O, Pellet O, et al. (2010) Pseudomyxoma peritonei: role of 18F-FDG PET in preoperative evaluation of pathological grade and potential for complete cytoreduction. Eur J Surg Oncol 36(3):315–323
24. Cabral FC, Krajewski KM, Kim KW, Ramaiya NH, Jagannathan JP (2013) Peritoneal lymphomatosis: CT and PET/CT findings and how to differentiate between carcinomatosis and sarcomatosis. Cancer Imaging 13:162–170
25. Buchpiguel CA (2011) Current status of PET/CT in the diagnosis and follow up of lymphomas. Rev Brasileira Hematol Hemoter 33(2):140–147
26. Karam M, Feustel PJ, Vera CD, Nazeer T (2011) Features of large cell transformation of indolent lymphomas as observed on sequential PET/CT. Nucl Med Commun 32(3):177–185
27. Oei TN, Jagannathan JP, Ramaiya N, Ros PR (2010) Peritoneal sarcomatosis versus peritoneal carcinomatosis: imaging findings at MDCT. AJR Am J Roentgenol 195(3):W229–W235
28. Wang B, Thomas R, Moskovic E, Benson C, Linch M (2013) Fistulation as a complication of intra-abdominal soft-tissue sarcomas; a case series. J Radiol Case Rep 7(6):15–21
29. Lee WK, Van Tonder F, Tartaglia CJ, et al. (2012) CT appearances of abdominal tuberculosis. Clin Radiol 67(6):596–604
30. Akhan O, Pringot J (2002) Imaging of abdominal tuberculosis. Eur Radiol 12(2):312–323
31. Leder RA, Low VH (1995) Tuberculosis of the abdomen. Radiol Clin N Am 33(4):691–705
32. Pereira JM, Madureira AJ, Vieira A, Ramos I (2005) Abdominal tuberculosis: imaging features. Eur J Radiol 55(2):173–180
33. Jeffry L, Kerrou K, Camatte S, et al. (2003) Peritoneal tuberculosis revealed by carcinomatosis on CT scan and uptake at FDG-PET. BJOG 110(12):1129–1131
34. Zhuang H, Pourdehnad M, Lambright ES, et al. (2001) Dual time point 18F-FDG PET imaging for differentiating malignant from inflammatory processes. J Nucl Med 42(9):1412–1417
35. Levy AD, Rimola J, Mehrotra AK, Sobin LH (2006) From the archives of the AFIP: benign fibrous tumors and tumorlike lesions of the mesentery: radiologic-pathologic correlation. Radiographics 26(1):245–264
36. Burke AP, Sobin LH, Shekitka KM, Federspiel BH, Helwig EB (1990) Intra-abdominal fibromatosis. A pathologic analysis of 130 tumors with comparison of clinical subgroups. Am J Surg Pathol 14(4):335–341
37. Azizi L, Balu M, Belkacem A, et al. (2005) MRI features of mesenteric desmoid tumors in familial adenomatous polyposis. AJR Am J Roentgenol 184(4):1128–1135
38. Basu S, Nair N, Banavali S (2007) Uptake characteristics of fluorodeoxyglucose (FDG) in deep fibromatosis and abdominal desmoids: potential clinical role of FDG-PET in the management. Br J Radiol 80(957):750–756
39. Makis W, Ciarallo A, Abikhzer G, Stern J, Laufer J (1010) Desmoid tumour (aggressive fibromatosis) of the colon mimics malignancy on dual time-point 18F-FDG PET/CT imaging. Br J Radiol 2012(85):e37–e40
40. Li X, Yu J, Fang S, Xing X, Zhao J (2014) Desmoplastic small round cell tumor: a case report and review of the literature. World J Surg Oncol 12(1):9
41. Tateishi U, Hasegawa T, Kusumoto M, et al. (2002) Desmoplastic small round cell tumor: imaging findings associated with clinicopathologic features. J Comput Assist Tomogr 26(4):579–583
42. Zhang WD, Li CX, Liu QY, et al. (2011) CT, MRI, and FDG-PET/CT imaging findings of abdominopelvic desmoplastic small round cell tumors: correlation with histopathologic findings. Eur J Radiol 80(2):269–273
43. Thomas R, Rajeswaran G, Thway K, et al. (2013) Desmoplastic small round cell tumour: the radiological, pathological and clinical features. Insights Imaging 4(1):111–118
44. Attanoos RL, Gibbs AR (1997) Pathology of malignant mesothelioma. Histopathology 30(5):403–418
45. Kebapci M, Vardareli E, Adapinar B, Acikalin M (2003) CT findings and serum ca 125 levels in malignant peritoneal mesothelioma: report of 11 new cases and review of the literature. Eur Radiol 13(12):2620–2626
46. Banayan S, Hot A, Janier M, et al. (2006) Malignant mesothelioma of the peritoneum as the cause of a paraneoplastic syndrome: detection by 18F-FDG PET. Eur J Nucl Med Mole Imaging 33(6):751
47. Cao Q, Lu M, Heath J, et al. (2012) 18F-FDG PET/CT in a recurrent diffuse malignant peritoneal mesothelioma. Clin Nucl Med 37(5):492–494
48. Ponce Lorenzo J, Gimenez Ortiz A, Aparisi Aparisi F, Fleitas Kanonnikoff T, Montalar Salcedo J (2007) Peritoneal mesothelioma: an inusual clinical presentation in a patient without exposure to asbestos. Anal Med Interna (Madrid, Spain: 1984) 24(2):81–83
49. Armato SG 3rd, Labby ZE, Coolen J et al (2013) Imaging in pleural mesothelioma: a review of the 11th International Conference of the International Mesothelioma Interest Group. Lung Cancer 82(2):190–196.
50. Tan C, Barrington S, Rankin S, et al. (2010) Role of integrated 18-fluorodeoxyglucose position emission tomography-computed tomography in patients surveillance after multimodality therapy of malignant pleural mesothelioma. J Thorac Oncol 5(3):385–388
51. Yildirim H, Metintas M, Entok E, et al. (2009) Clinical value of fluorodeoxyglucose-positron emission tomography/computed tomography in differentiation of malignant mesothelioma from asbestos-related benign pleural disease: an observational pilot study. J Thorac Oncol 4(12):1480–1484
52. Sharif S, Zahid I, Routledge T, Scarci M (2011) Does positron emission tomography offer prognostic information in malignant pleural mesothelioma? Interact Cardiovasc Thorac Surg 12(5):806–811
53. Malpica A, Sant'Ambrogio S, Deavers MT, Silva EG (2012) Well-differentiated papillary mesothelioma of the female peritoneum: a clinicopathologic study of 26 cases. Am J Surg Pathol 36(1):117–127
54. Park JY, Kim KW, Kwon HJ, et al. (2008) Peritoneal mesotheliomas: clinicopathologic features, CT findings, and differential diagnosis. AJR Am J Roentgenol 191(3):814–825
55. Costanzo L, Scarlata S, Perrone G, et al. (2014) Malignant transformation of well-differentiated papillary mesothelioma 13 years after the diagnosis: a case report. Clin Respir J 8(1):124–129
56. Kim JS, Lee HJ, Woo SK, Lee TS (1997) Peritoneal inclusion cysts and their relationship to the ovaries: evaluation with sonography. Radiology 204(2):481–484

57. Canbay E, Ishibashi H, Sako S, et al. (2013) Late recurrence of benign multicystic peritoneal mesothelioma complicated with an incisional hernia. Case Rep Surg 2013:903795
58. Singh A, Chatterjee P, Pai MC, Chacko RT (2013) Multicystic peritoneal mesothelioma: not always a benign disease. Singap Med J 54(4):e76–e78
59. Shmueli E, Leider-Trejo L, Schwartz I, Aderka D, Inbar M (2001) Primary papillary serous carcinoma of the peritoneum in a man. Ann Oncol 12(4):563–567
60. Chiou SY, Sheu MH, Wang JH, Chang CY (2003) Peritoneal serous papillary carcinoma: a reappraisal of CT imaging features and literature review. Abdom Imaging 28(6):815–819
61. Morita H, Aoki J, Taketomi A, Sato N, Endo K (2004) Serous surface papillary carcinoma of the peritoneum: clinical, radiologic, and pathologic findings in 11 patients. AJR Am J Roentgenol 183(4):923–928
62. Wang PH, Liu RS, Li YF, Ng HT, Yuan CC (2000) Whole-body PET with (fluorine-18)-2-deoxyglucose for detecting recurrent primary serous peritoneal carcinoma: an initial report. Gynecol Oncol 77(1):44–47
63. Hardman WJ 3rd, Majmudar B (1996) Leiomyomatosis peritonealis disseminata: clinicopathologic analysis of five cases. South Med J 89(3):291–294
64. Al-Talib A, Tulandi T (2010) Pathophysiology and possible iatrogenic cause of leiomyomatosis peritonealis disseminata. Gynecol Obstetr Invest 69(4):239–244
65. Lamarca M, Rubio P, Andres P, Rodrigo C (2011) Leiomyomatosis peritonealis disseminata with malignant degeneration. A case report. Eur J Gynaecol Oncol 32(6):702–704
66. Georgiades CS, Neyman EG, Francis IR, Sneider MB, Fishman EK (2002) Typical and atypical presentations of extramedullary hemopoiesis. AJR Am J Roentgenol 179(5):1239–1243
67. Holden C, Hennessy O, Lee WK (2006) Diffuse mesenteric extramedullary hematopoiesis with ascites: sonography, CT, and MRI findings. AJR Am J Roentgenol 186(2):507–509
68. Patnana M, Sevrukov AB, Elsayes KM, et al. (2012) Inflammatory pseudotumor: the great mimicker. AJR Am J Roentgenol 198(3):W217–W227
69. Uysal S, Tuncbilek I, Unlubay D, et al. (2005) Inflammatory pseudotumor of the sigmoid colon mesentery: US and CT findings (2004:12b). Eur Radiol 15(3):633–635
70. Chaulagain CP, Comenzo RL (2013) New insights and modern treatment of AL amyloidosis. Curr Hematol Malig Rep 8(4):291–298
71. Coulier B, Montfort L, Doyen V, Gielen I (2010) MDCT findings in primary amyloidosis of the greater omentum and mesentery: a case report. Abdom Imaging 35(1):88–91
72. Kim MS, Ryu JA, Park CS, et al. (2008) Amyloidosis of the mesentery and small intestine presenting as a mesenteric haematoma. Br J Radiol 81(961):e1–e3
73. Pickhardt PJ, Bhalla S (2005) Unusual nonneoplastic peritoneal and subperitoneal conditions: CT findings. Radiographics 25(3):719–730